sustainability

MDPI

Article

Design and Implementation of a MHz Frequency Transformer with a Ferromagnetic Fluid Core

Erol Kurt [1,*] and Sude Hatem [2]

[1] Department of Electrical and Electronics Engineering, Technology Faculty, Gazi University, Besevler, Ankara 06500, Turkey
[2] Department of Electrical and Electronics Engineering, Faculty of Engineering, Cankaya University, Ankara 06690, Turkey
* Correspondence: ekurt@gazi.edu.tr

Abstract: Design and optimization of a magnetic fluid cored transformer are studied for high frequency applications. An easy and cheap fluid core is designed and used to decrease the eddy current and loses, thereby low conducting and paramagnetic features are added. The core exhibits both fluid and solid characteristics exerting high frequency modes in the fluid and low current due to the iron powder inside. The finite element analysis simulations are performed via COMSOL Multi-physics package for different mass fractions of iron powder. The maximum peak-to-peak voltage and power are found as 526 mV and 188.8 mW at 12 MHz from the simulations. 3D patterns prove that the magnetic flux and magnetization exhibit turbulence in the core, thereby localized magnetic values indicate an arbitrary attitude for various frequencies. Optimum mass fraction is found as 0.7, which is parallel with experimental results. The transformer operates between 11 MHz and 13.5 MHz optimally.

Keywords: transformer; magnetic core; magnetic fluid; high frequency; MHz

Citation: Kurt, E.; Hatem, S. Design and Implementation of a MHz Frequency Transformer with a Ferromagnetic Fluid Core. *Sustainability* **2023**, *15*, 23. https://doi.org/10.3390/su15010023

Academic Editors: Xiaodong Sun and Shuhua Fang

Received: 20 October 2022
Revised: 5 December 2022
Accepted: 15 December 2022
Published: 20 December 2022

1. Introduction

The most effective distribution transformers run with a loss of about 3% of the electricity they transmit, except for interruptions for maintenance and breakdown. In order to lower operational costs and energy losses, the industrial divisions are continually looking into innovative techniques and technologies. Since the development of transformers, the choice of appropriate materials for the manufacture of the core has been carefully addressed since it has a significant impact on the performance of the transformers. With an appropriate core material, losses at high flux density (B) can be minimized and the transformer can run at the desired frequencies (f). Magnetic elements play a considerable role in accomplishing the mentioned features. Electrical components, transformers and coils operate well at higher operating frequencies (kHz and MHz) with smaller dimensions thanks to the development of high-frequency switching components. Though, there are additional losses associated with these tiny dimensions. In order to minimize parasitic output and maximize efficiency in high operating frequency devices, magnetic element selection is important. The transformer will be primarily protected from overheating due to core loss by selecting the proper core. For the optimal design, a balance between a number of material characteristics, such as resistivity, magnetic saturation, and electrical permeability, is essential.

The power-frequency logarithmic graph for transformers with various core materials currently in use in literature and industry is shown in Figure 1 [1]. This graph shows that the frequency (f) and power (P) characteristics of cores made from nanocrystalline materials are uniformly distributed, while cores made of SiFe material are preferred at low frequencies and amorphous cores are chosen at mid-low frequencies and relatively low powers. However, ferrite structures are similar to amorphous in terms of power while being

able to operate at higher frequencies (about 14 kHz). Applications involving nanocrystals may include transformers with 100 kHz operating frequencies. More magnetic materials have been introduced for various applications with rising operating frequency. Depending on the application and system topology, magnetic core structures change. While several grades of steel lamination were employed in the past, adding 4–5% silicon to steel has the potential to minimize eddy currents and hysteresis losses while also improving the performance and efficiency of the transformer [2,3]. The four primary categories of core materials for commercially available transformers are amorphous materials, iron alloys, iron powders and soft magnetic ferrites.

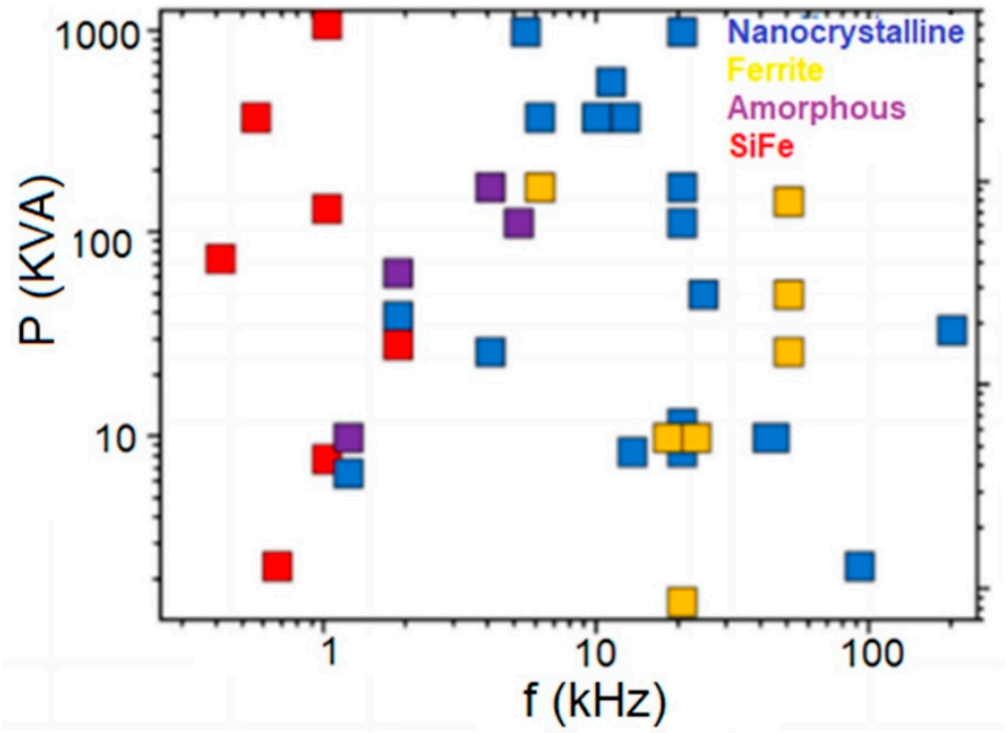

Figure 1. Power-frequency characteristics of soft materials [1].

By examining these classes briefly, it is seen that the most popular example in the ferrous alloys category is silicon steel material (SiFe). This material has high saturation and flux density at low frequencies. However, for such materials, eddy current losses are significant at high frequencies (kHz and MHz). In high frequency transformers (e.g., Planar transformer), it is desirable that the structure has low conductivity and high permeability. In addition, the structure must have high resistance at high frequencies in order to decrease the eddy current losses. This fact declares that silicon steel materials are not appropriate to be used as a core in high-frequency devices such as planar transformers and it is common for low-frequency (Hz) applications, as can be seen from Figure 1.

Amorphous materials with their high electrical resistance, low core losses and high magnetic permeability are preferred for medium-high frequency (kHz) applications. The study of fundamental materials is significantly impacted by global efforts to conserve energy and environmental issues. In this sense, amorphous structures are good examples [4]. Magnetic flux density (B), core loss, magnetic permeability, and dynamic magnetic properties under different operating temperatures in hardened Fe78Si13B9 amorphous alloy cores are systematically given in [5] and properties of similar magnetic core materials are given in [6]. Powder core materials, such as nanoscale iron powder structures, are employed at relatively high frequencies.

Generally, power electronic device efficiency and power density are greatly influenced by the magnetic components. Core losses are minimal for some components, such as DC

filter coils, but they account for a notable portion of the total losses for transformers and AC coils, hence these losses should be considered [7].

Another important characteristic that affects the operation of transformers is the geometry. The assumption of homogeneous magnetic flux density within the transformer core has been used as a common approach in designs. This approach simplifies the estimation of core losses. Regardless of the size and shape of the core, the spatial distribution of the core losses is homogeneous as a linear function of the flux density field, so the geometric impacts on the overall core loss can be disregarded. For example, as shown in Figure 2—since the toroidal and rectangular cores have the same excitation, the same cross-sectional area (A) and the same flux path (l_m)—it is assumed that their total losses will be the same.

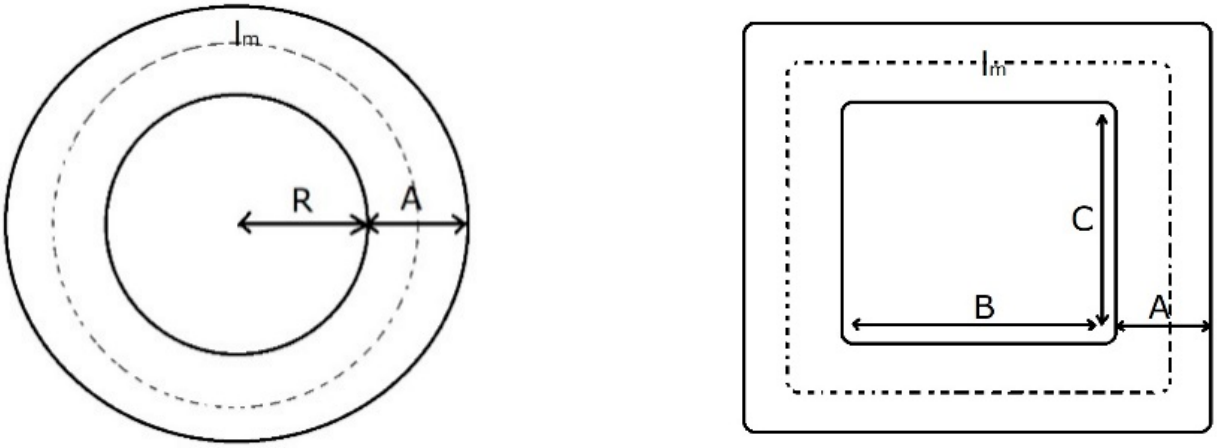

$$l_m = 2(R + \frac{1}{2}A)\pi \qquad l_m = 2(\frac{\pi}{2}A + B + C)$$

Figure 2. Commonly used core geometries [8].

Where R is the inner radius of the toroidal core, and B and C are the inner sides of the rectangular core. However, this assumption is wrong considering the shape and structure of the core [8]. The impact of core shape on various cores is examined in a variety of research in the literature. For example, for industrial distribution transformers in the power range, the measurements performed in [9] quantitatively examined the impact of core geometry on no-load losses (16–20 MVA). Again, [10] experimentally reported the effect of different geometry structures on the total losses in toroidal cores. To estimate the areas and loss distributions in discrete and solid rectangular and toroidal cores, partial differential equations' analytical formulation and methods are addressed in [11]. In another study, the effect of harmonics at high excitation amplitudes was analyzed by the finite element method [12].

In another study, analyses were conducted on various geometries by electromagnetic simulation and studies were conducted on their accuracy [13]. By modeling the distribution of magnetic field on the core structures and created losses, detailed analyses were conducted [8]. Additionally, in the models derived in this study, sample core loss measurements with any geometry were made and a comparison was made between transformer cores with different geometries manufactured from the same material by the same method. In comparison, it has been observed that the magnetic core volume can be reduced at high frequency. However, the use of soft magnetic materials with low core losses such as amorphous and ferrous alloys with high permeability has been found to be more appropriate compared to other materials, and the use of amorphous and ferrous alloys has been suggested for designing high-frequency transformers [14,15]. The use of frequency-matched quality core material, the efficiency of the cooling medium and methods significantly affect

the flux level formed. In the study conducted in [16], three methods were considered. The methodology has been proposed to raise the transformer's level of efficiency and safety of operation. The majority of the core losses are made up of hysteresis and eddy current losses. Only a small part of these losses is permanent [17,18]. There are two main approaches to figure out these losses. Utilizing the Steinmetz formula to determine the core losses is one of these techniques [19,20]. For example, the developed Steinmetz formula is used in order to examine the cores of high-frequency transformers and determine the core loss characteristics of various materials in a three-dimensional manner [19]. The Steinmetz formula is developed using the notion of flux waveform coefficients, suggested in [21] by examining properties of losses under various excitation forms.

The loss separation approach is another suggestion. According to this method, core losses are divided into eddy current loss and hysteresis loss [22]. In a study conducted with this method, the characteristics of the core's hysteresis losses under DC bias are investigated [23]. Large inaccuracies frequently occur when estimating the real losses of transformers. Since the traditional iron core loss calculation approach assumes that the magnetic field distribution in the iron core is homogenous. Calculation of core losses by the finite element method using computer simulation has been a valid method all over the world [24,25]. The iron core loss curve is subtracted from the magnetic flux density, and the core losses are then determined by adding together all unit losses. In this regard, appropriate results have been obtained with finite elements in calculating the core loss under DC condition [26].

With the developments in the computer industry, an increase has been observed in the designs of chip and on-board transformers. Planar transformers have especially been widely used recently. In such systems, in order to achieve maximum efficiency, design optimization of all possible additional losses should be made [27]. There are various restrictions placed on traditional wire-wound magnetic components as a result of the increased losses that come with high operating frequency. When the operating frequency is raised from KHz to MHz, these losses get significantly worse. Planar transformers are considered a solution in this situation. Planar systems rather than traditional wire winding systems are employed to reduce high frequency losses and parasitic limits. This type of transformer has become more popular among designers because of its great thermal stability, high reliability, low leakage inductance and high frequency ranges (MHz). Studies have been made to increase the current carrying capacity of the windings on the high frequency planar transformer application, and the special problems arising from the parallel winding have been modeled by considering a one-dimensional field model [27]. Similarly, the properties of planar magnetic structures used in medium power (10–500 W) applications were reviewed and the properties of planar systems were investigated [28]. The details of the negative factors such as ohmic loss and parasitic capacitance of on-chip transformers with different magnetic cores investigated are covered in detail [29]. In addition to the aforementioned factors, research has revealed that core loss of "solid" magnetic cores has a substantial impact on the performance of transformers. There is a detailed discussion of a few core loss remedies [30,31]. In some studies, prototypes of ferromagnetic fluid (ferrofluid) core transformers have been presented in the literature, the structure and experimental results of ferrofluid core microtransformers have been revealed [32]. In these studies, a significantly fewer number of coils and magnetic fluid are used. In addition, the applied frequency is in the high band and the magnetic fluid used is oil-based [33]. In contrast, different types of magnetic fluids and larger quantities of magnetic fluids in the same type of transformer can exhibit very different properties at relatively low operating frequencies.

In a study conducted in this direction, Fe_3O_4 oil-based nanofluids, which can be used in the core of planar systems, were formed from a mixture of Fe_3O_4 nanoparticles, surfactant, diesel oil and polydimethylsiloxane (PDMS) [30]. A small-sized magnetic liquid-core prototype transformer was designed in [34] and the output characteristics of this transformer at different frequency values were investigated. The magnetic fluid used as a core in the aforementioned study is an iso-paraffin-based fluid prepared in an industrial

environment. The number of windings of the prototype transformer, which has 1 mL of magnetic fluid in its core, has been adjusted by winding according to its electrical resistance. When the test results of the designed transformer are examined, it is observed that the output voltage of the transformer decreases rapidly at high frequencies such as 1 MHz.

The main innovation of the present work is that we aim to design and construct a transformer working with a very cheap ferro-fluid structure combined with iron dusts and engine oil in its core having special geometry, which has not been worked experimentally and theoretically before. In this context, we explore the characteristic features of the new transformer for the first time to our knowledge and prove that it gives both solid and liquid features depending on the mass fraction of the ferromagnetic material. It will be also proven that there exist a certain mass fraction leading the maximum power at the terminals of secondary windings. Moreover, for the first time to our knowledge, we operate the transformer under MHz range and find that the transformer works well under such a high frequency regime. Due to its low electrical conductivity and superparamagnetic oil-base qualities, the ferrofluid core transformer is a suitable candidate for a prototype solution to eddy currents and hysteresis losses (core losses). Two significant elements affecting the performance of transformers are their weight and rate of magnetization. In the core of electromagnetic systems used for specific applications, magnetic liquid materials may therefore be favored. The numerical study and simulation process for designing a liquid core transformer is evaluated in [29]. The designed magnetic fluid core transformer (MFT) actually has electrical characteristics and output characteristics that are similar to those of solid core transformers used in industry. It is preferred in a variety of fields and applications, including the defense industry and medicine, because of its high efficiency, longer lifespan, small size, light weight, and high core magnetization. The ferrofluid that serves as the core of the MFT must be created in phases. Consequently, a simpler method that is quicker and less expensive may be preferred for the manufacturing of ferrofluid. In this study, a straightforward, affordable, and effective method for using ferrofluid as a transformer core is presented and put into practice through experimental tests.

In Section 2, the theoretical background of the proposed transformer model containing a liquid core is explained and the mathematical model is defined. The definition of the ferrofluid used as MFT's core and numerical simulation results for various concentrations of nanoparticles floated in an oil base are presented in detail in Section 3. The test and experimental setup belonging to the system are presented in Section 4. The experimental results of the designed MFT and discussion are explained in Section 5. Finally, the conclusion of the current study is presented in Section 6.

2. Theoretical Background

In high frequency applications, electromagnetic fields have the function of carrying energy in all electromagnetic environments. Therefore, both precise analytical and numerical analyses of the electromagnetic fields are important tasks for the examination of the properties of these devices and systems. The magnetic dipoles in a ferrofluid are pointed in the same direction in the presence of an external magnetic field (H). Without a net magnetization, they are otherwise randomly orientated. Large amplitude surface waves are produced when a fluid is agitated, creating a complicated fluid motion. Due to the turbulence, the magnetic dipoles' direction varies during the agitation, creating abrupt changes in the magnetic flux. When a coil is wrapped around the container, this action results in the outside of the container experiencing an electromotive force (EMF). The primary distinction between a ferrofluid and a solid core is that a ferrofluid's turbulent motion causes it to have an endless number of modes. The H source should first be modeled in order to develop the mathematical model. Following that, the magnetization body forces are assessed, and the magnetic field is computed. The flow in the liquid core is next examined. According to the

mathematical model in the windings, electric currents are a static issue for the electric field inside the coil (magnetic field source).

$$\nabla \cdot (\sigma \nabla V_e) = 0, \tag{1}$$

where, V_e [V] is the electrokinetic potential. The terminals of each coil specify Dirichlet boundary conditions (voltage at one end, ground at the other) depending on the power scheme. σ [S/m] defines the electric conductivity. After calculating the current density, the static magnetic field solver solves the following expressions using Ampere's Law and Maxwell's equations:

$$\nabla \times \vec{H} = \vec{J}_e + \vec{J_o} \tag{2}$$

$$\nabla \cdot \vec{B} = 0 \tag{3}$$

$$\nabla \cdot \vec{D} = \rho \tag{4}$$

Here, $\vec{H}(x, y, z)$ [A/m] is the magnetic field strength, $\vec{B}(x, y, z)$ [T] is the magnetic flux density, $\vec{J}_e$ [A/m^2] is eddy current density and $\vec{J_o}$ [A/m^2] is the external current density, $\vec{D}$ [C/m^2] is defined as the electric flux density and ρ [C/m^3] is the electrical charge density. The magnetic flux density:

$$\vec{B} = \mu_r \, \mu_0 \, \vec{H} \tag{5}$$

where $\mu_r(x, y, z)$ is the relative permittivity and $\mu_0 = 4\pi 10^{-7}$ [H/m]. The system calculates the moment about the x, y, z axis using the Lorentz force:

$$T = \int \vec{r} \times \left(\vec{J} \times \vec{B} \right) dv \tag{6}$$

Here T represents the moment. J [A/m^2] and r are the current density and displacement vectors in the rotation axis, respectively. Boundary condition of electrical insulation is,

$$n \cdot \vec{J} = 0 \tag{7}$$

n is the outward normal. The resulting current density is defined as an external field source to the magnetic field problem. The analysis of inductances is based on the mathematical model for the magnetic field:

In copper windings and in free space:

$$\nabla \times \left(\mu_0^{-1} \mu_r^{-1} \nabla \times \vec{A} \right) = J_e \tag{8}$$

In ferrofluid core:

$$\nabla \times \left(\mu_0^{-1} \mu_r^{-1} \nabla \times \vec{A} - \vec{M} \right) = 0 \tag{9}$$

where, $\vec{A}$ [T.m] is the magnetic vector potential and $\vec{M}$ [A/m] is the magnetization of the magnetic fluid and with analytical formula of the magnitude:

$$M = \alpha \arctan(\beta H) \tag{10}$$

Here, α and β are the experimental constants chosen to exactly match the magnetic fluid's experimental magnetization properties. As theoretical equations,

- Conservation of momentum:

$$\rho \left(\vec{u} \cdot \nabla \right) \vec{u} = \nabla \cdot \left[-pI + \eta \left((\nabla u) + (\nabla u)^T \right) \right] + f_{mg} - \rho g \tag{11}$$

- Mass conservation:

$$\nabla \cdot \vec{u} = 0 \tag{12}$$

- Turbulent kinetic energy transportation:

$$\rho \vec{u} \cdot \nabla k = \nabla \cdot [(\eta + \sigma_k \eta_T)\ \nabla k] + \eta_T P(u) - \beta \rho k \omega \tag{13}$$

- Turbulent frequency transportation:

$$\rho \vec{u} \cdot \nabla \omega = \nabla . [(\eta + \sigma_\omega \eta_T)\ \nabla \omega] + \propto \omega\ \eta_T P(u)/k - \beta \rho \omega^2 \tag{14}$$

The ferro-fluid behavior is explained by solving the formulas together. Here u [m/s] is the velocity, p [N/m^2] defines the pressure, ρ [kg/m^3] is the mass density, g [m/s^2] is the gravitational acceleration, I is the unity matrix, and η [s^{-1}] is the dynamic viscosity.

$$\vec{f_{mg}} = \mu_0 \left(\vec{M} \cdot \nabla \right) \vec{H} \tag{15}$$

Here $\vec{f_{mg}}$ [N/m^3] is defined as magnetization external force [6]. The pressure and turbulent viscosity are given by,

$$P(u) = \nabla \cdot \vec{u} \left[\ \nabla \cdot \vec{u} + \left(\nabla \cdot \vec{u} \right)^T \right] \tag{16}$$

$$\eta_T = \rho k / \omega \tag{17}$$

Here, $\omega \left[\mathrm{m}^2/\mathrm{s}^3 \right]$ is the turbulent frequency and k [J/m^3] is the turbulent kinetic energy. The modeled magnetic nanofluid, is considered as a Newtonian, homogeneous and isotropic fluid.

3. Simulation Results and Discussion

All designs of the MFT subjected to this article, are realized through COMSOL Multiphysics package program, which uses the three-dimensional finite element method. A transformer, in terms of modeling, essentially has a 3D shape. When used in the construction of electrical machines, the 3D finite element method enables extremely precise estimation of key design parameters such the encircled flux, current density, winding inductances, and the produced electromagnetic field. The responses of the system in various circumstances can be predicted ahead using the chosen program, provided the parameters of the materials and the boundary conditions are supplied correctly [7]. [Partial differential equations cannot be solved analytically for the vast majority of geometries and issues. Instead, an approximation of the equations can be built, usually based on various discretization techniques. These discretization techniques combine numerical model equations that may be solved numerically to approximate PDEs. The real solution to PDEs is approximated by solving the numerical model equations. Such approximations are computed using the finite element method (FEM) [15].

In order to define the considered ferro-fluid material properties of MFT's core, the characteristics and physical parameters given in Table 1 are applied and the *B-H* curve of the ferromagnetic particles is introduced to the defined material by adding a specific constitutive *B-H* relation. As a result, the magnetic field norm would need a definition depended on the *B-H* curve, hence reaching both properties of fluidity and ferromagnetism are possible. In order to design and evaluate magnetic body forces and observe the magnetic flux intensity of flow patterns of velocity field through the MFT's core, magnetic fields and computational fluid dynamics (CFD) modules are used physics in simulation program of Comsol Multi-Physics v5.6.

Table 1. Physical parameters of engine oil-based ferro-fluid used in simulation model.

Parameter	Description
Dynamic viscosity [Pa s]	0.15
Density [g/cm^3]	1.21–7.104
Heat capacity at constant pressure [J/(kg K)]	1.67
Thermal conductivity [W/mK]	0.176
Electrical conductivity [MS/m]	10^{-12}
Chemical composition of magnetic particle	Fe
Magnetic particle mean radius [μm]	70
Magnetic particles weight concentration	0.1–0.9
Operating frequency [MHz]	1–20

The issue is resolved using the Galerkin finite element technique (FEM). The model's newly added meshing sequence is calibrated using fluid dynamics for the ferrofluid core domain and general physics for the rest geometry of the MFT. Figure 3 shows the created mesh.

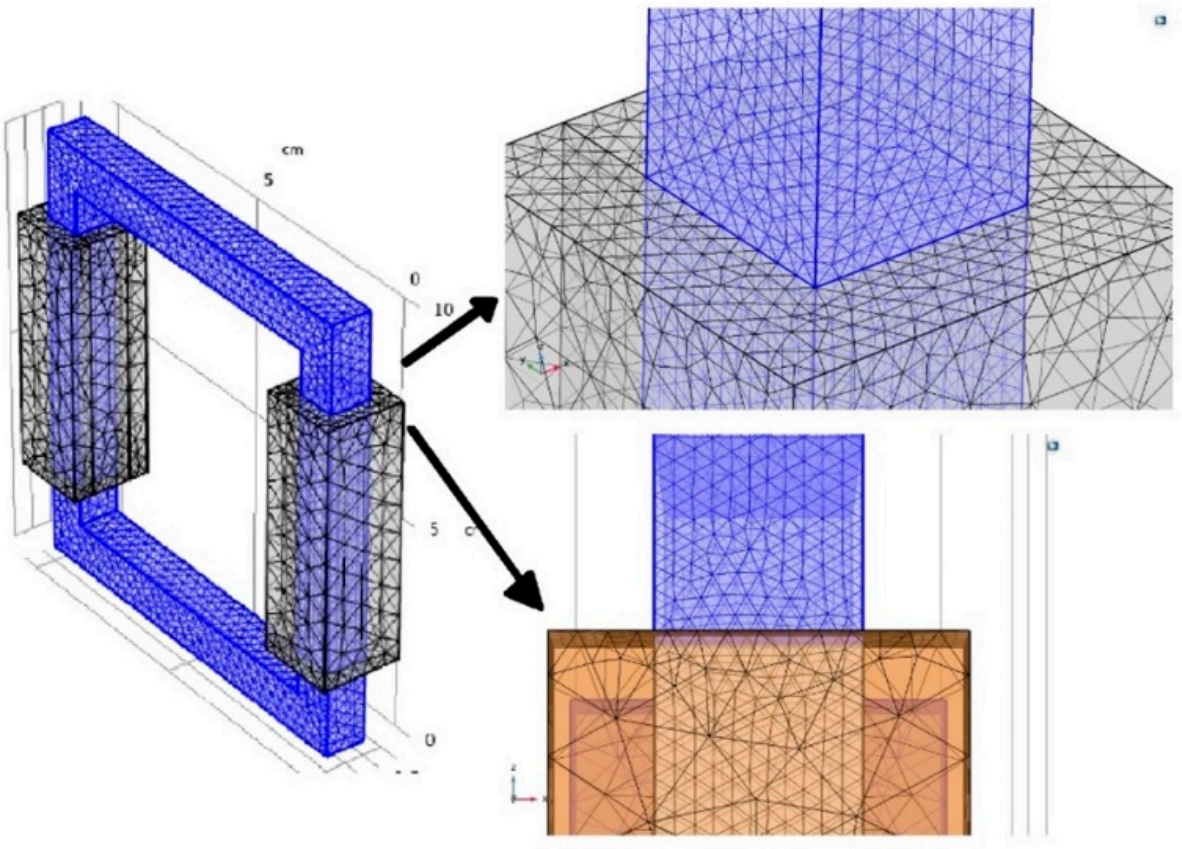

Figure 3. The meshed MFT structure.

The Equations (7)–(9) can be solved if the magnetic field source is identified. In the numerical simulations, the field is modeled using tetrahedral, quadratic vector elements. Because of the nonlinear behavior of the ferrofluid core, the algebraic problem relating to the FEM analysis is nonlinear. As a result, the MUMPS solver algorithm is preferred to improve sequential and parallel sparse numerical factorization performance by combining left-looking and right-looking super node approaches. According to various average mass concentration of dispersed nanoparticles, the density of mixture consisting of iron powder nanoparticles and engine oil is calculated and presented in Table 2.

Table 2. The magnetic nanoparticles and engine oil mixture density for various particles mass fractions.

Nanoparticles Concentration (φ_d) %	Mixture Density (ρ) [kg/m^3]
5	1218.87
10	1565.25
20	2258
30	2950.75
40	3643.5
50	4336.25
60	5029
70	5721.75
80	6414.5
90	7104.8

In the first phase of operation, in order to visualize the magnetic flux density produced, the simulation process is conducted for a MFT core with $\rho = 4336.25$ [kg/m^3] mixture density, which corresponds to about 50% nanoparticles mass fraction. The magnetic flux density spectrum and flowing flux of simulated MFT by three powering schemes are indicated in Figure 4 through flux lines. The first scenario is powering only the primary winding, the second scenario is powering only the secondary winding and the third one is powering both windings with additional flux excitation. The simulation results for the above-mentioned two processes are presented via graphics and plots.

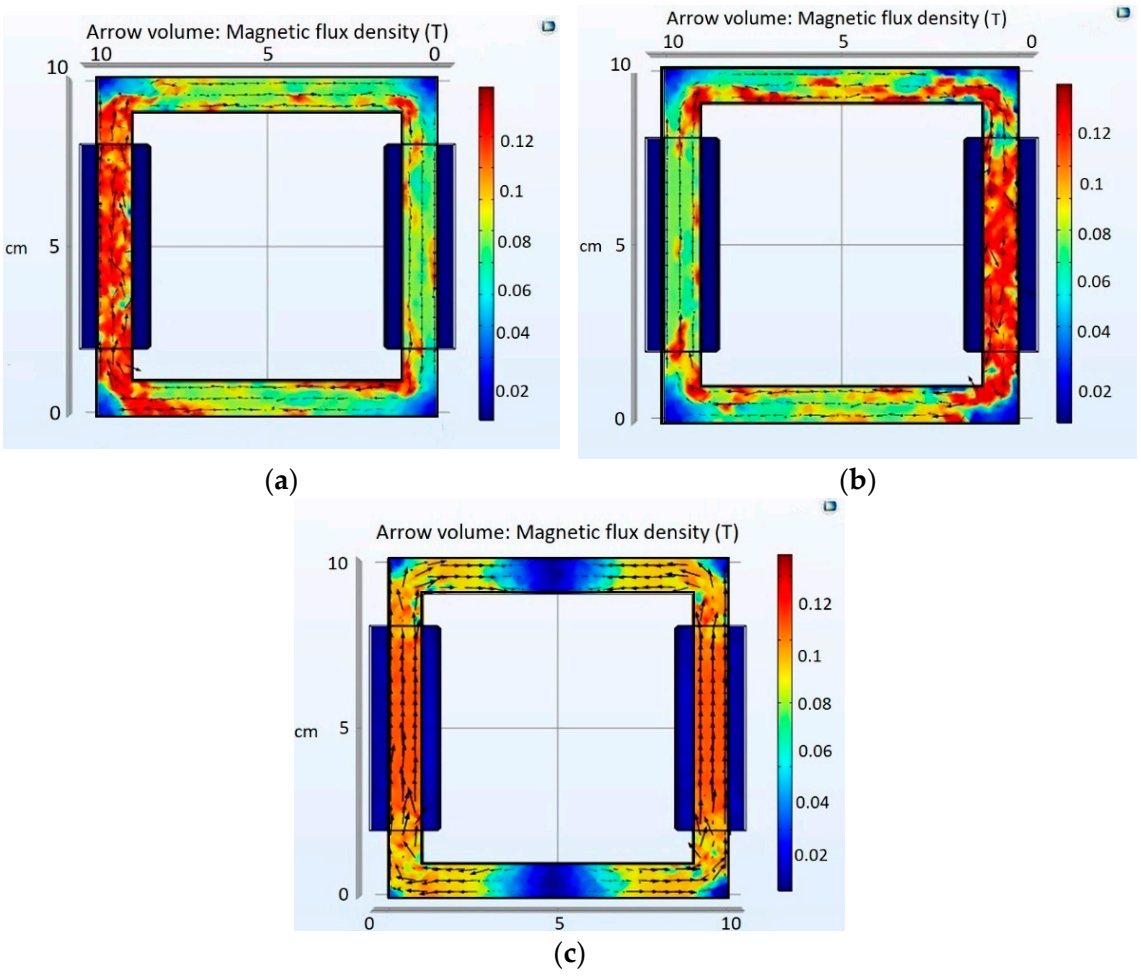

Figure 4. The flow of flux and the magnetic flux density spectrum: (**a**) Power is applied to the primary winding, (**b**) Power is applied to the secondary winding, and (**c**) Power is applied to both windings excited by the same current.

The color and size of the lines are proportional to the amount of magnetic flux density of the model. The published results show that instead of their random orientations, the magnetic dipoles in the ferrofluid are orientated in the same direction when no magnetic field is applied. Hence, no magnetization exists. When an external magnetic field is applied and a very small agitation is occurred in the fluid, a complicated fluid motion involving large amplitude surface waves occurs. This turbulent action changes the direction of the magnetic dipoles, which causes sudden changes in magnetic flux. The influence of the external magnetic body forces on magnetization of ferrofluid core is observed by numerical simulation. The magnetic field strength (H) and the magnetization norm (M) formed in designed MFT are given in Figures 5 and 6, respectively. As mentioned, the obtained results are admissible for the powering scheme illustrated.

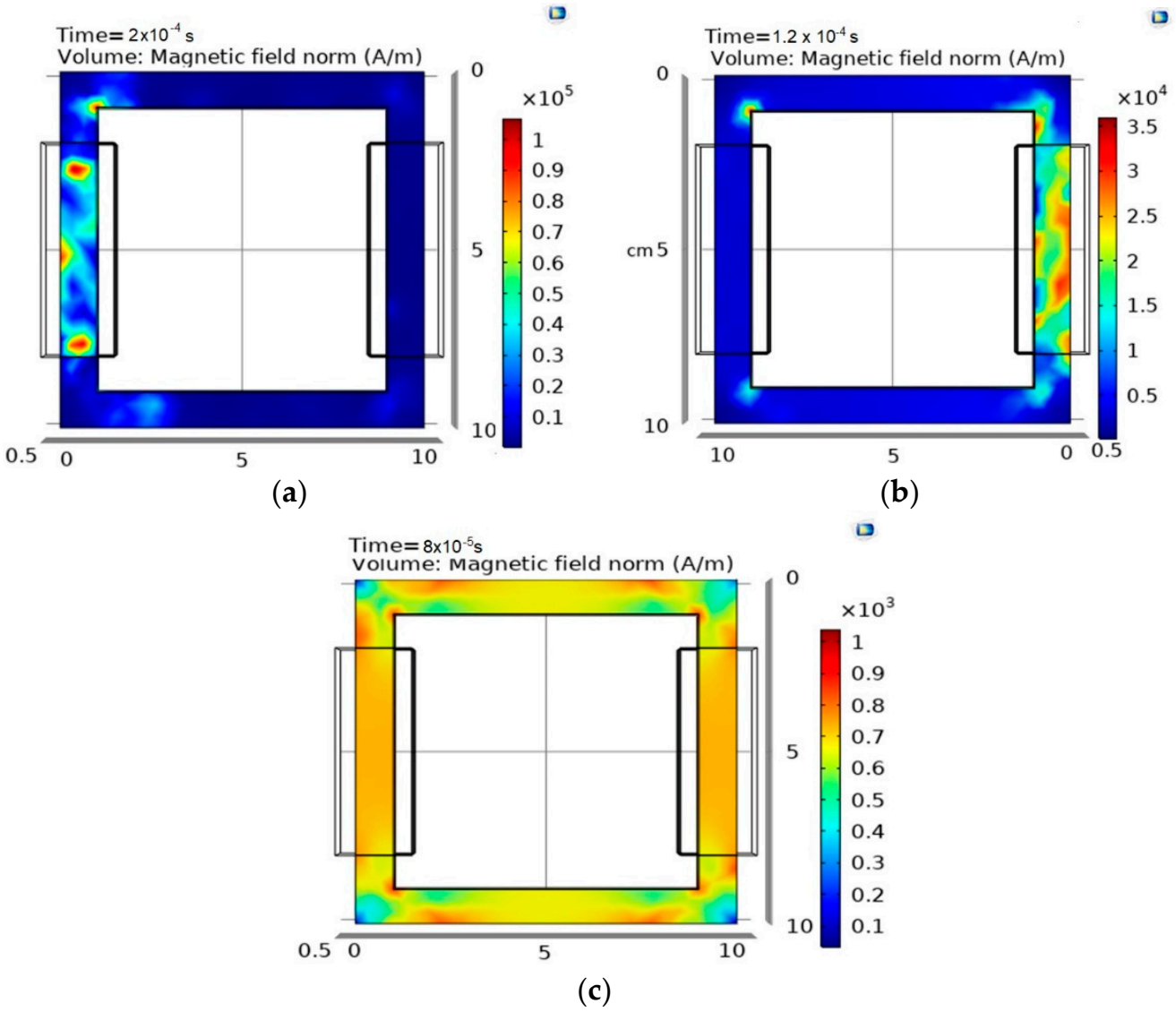

Figure 5. The magnetic field strength formed in designed MFT: (**a**) Power is applied to the primary winding, (**b**) Power is applied to the secondary winding, (**c**) Power is applied to both windings excited by the same current.

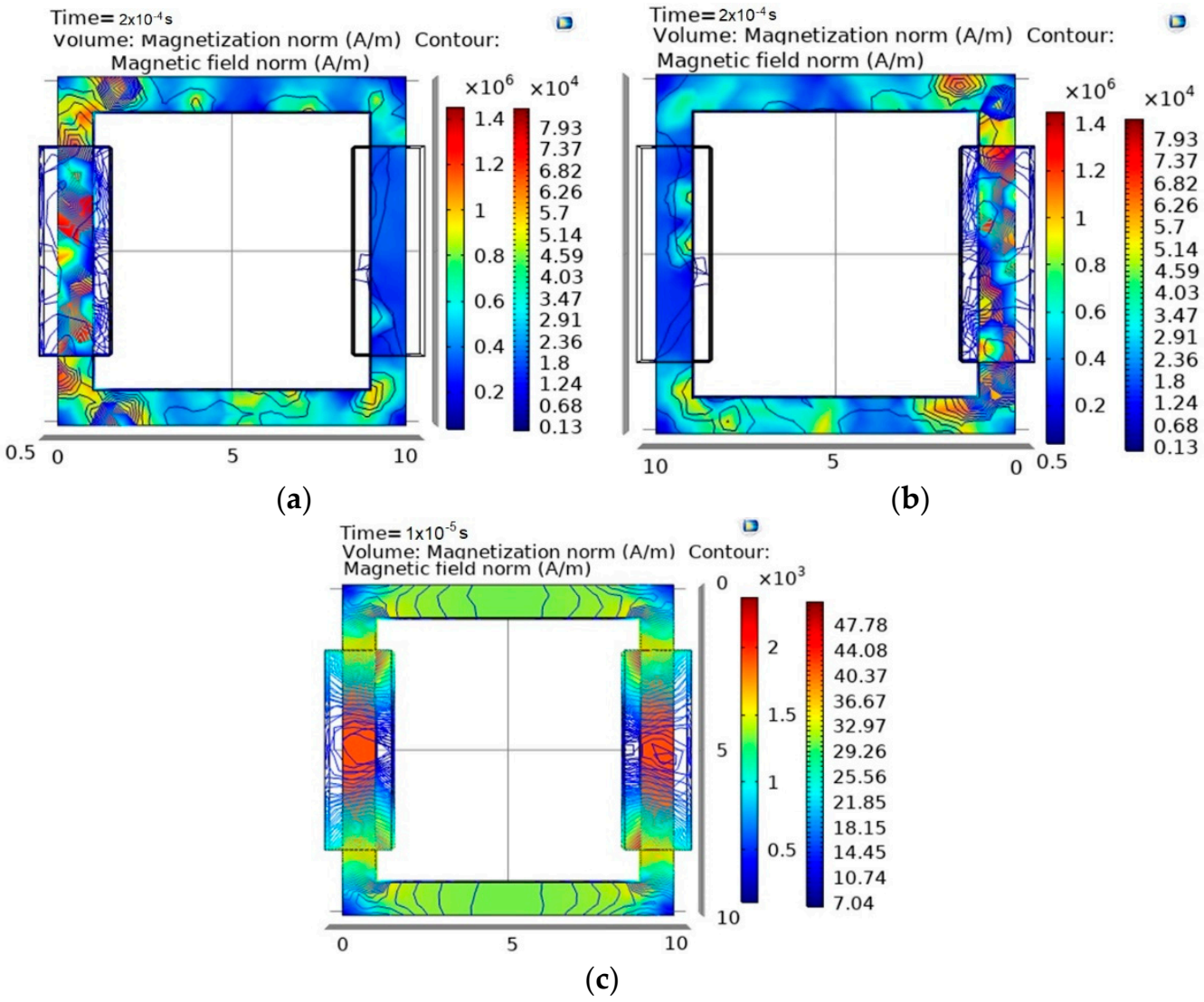

Figure 6. The magnetization in the designed MFT: (**a**) Power is applied to the primary winding, (**b**) Power is applied to the secondary winding, (**c**) Power is applied to both windings excited by the same current.

In order to obtain the results of magnetic fields and turbulent flow modules simultaneously, both physics are applied to the same study in simulation model. As a result, it is possible to observe the flow patterns created in MFT's core by applying magnetic forces. Stream tubes depict the flow field, and their color and size are related to the velocity module. It should be noticed that the mass concentration of the particles floating in fluids is constant for the simulation model. Therefore, the magnetization body forces that entrain the flow are not different. Figure 7 presents 3D views of the velocity field (v) and Figure 8 indicates the pressure (P) through the core as both physics are applied.

The magnetic flux densities and the flowing fluxes for primary winding excitation with an identical AC current are indicated through flux lines. Since the study is time dependent, the magnetic flux density produced is varying with respect to time. In this case, the MFT contains a core with 50% mass fraction of magnetic nanoparticles (ρ =4336.25 [kg/m^3] mixture density).

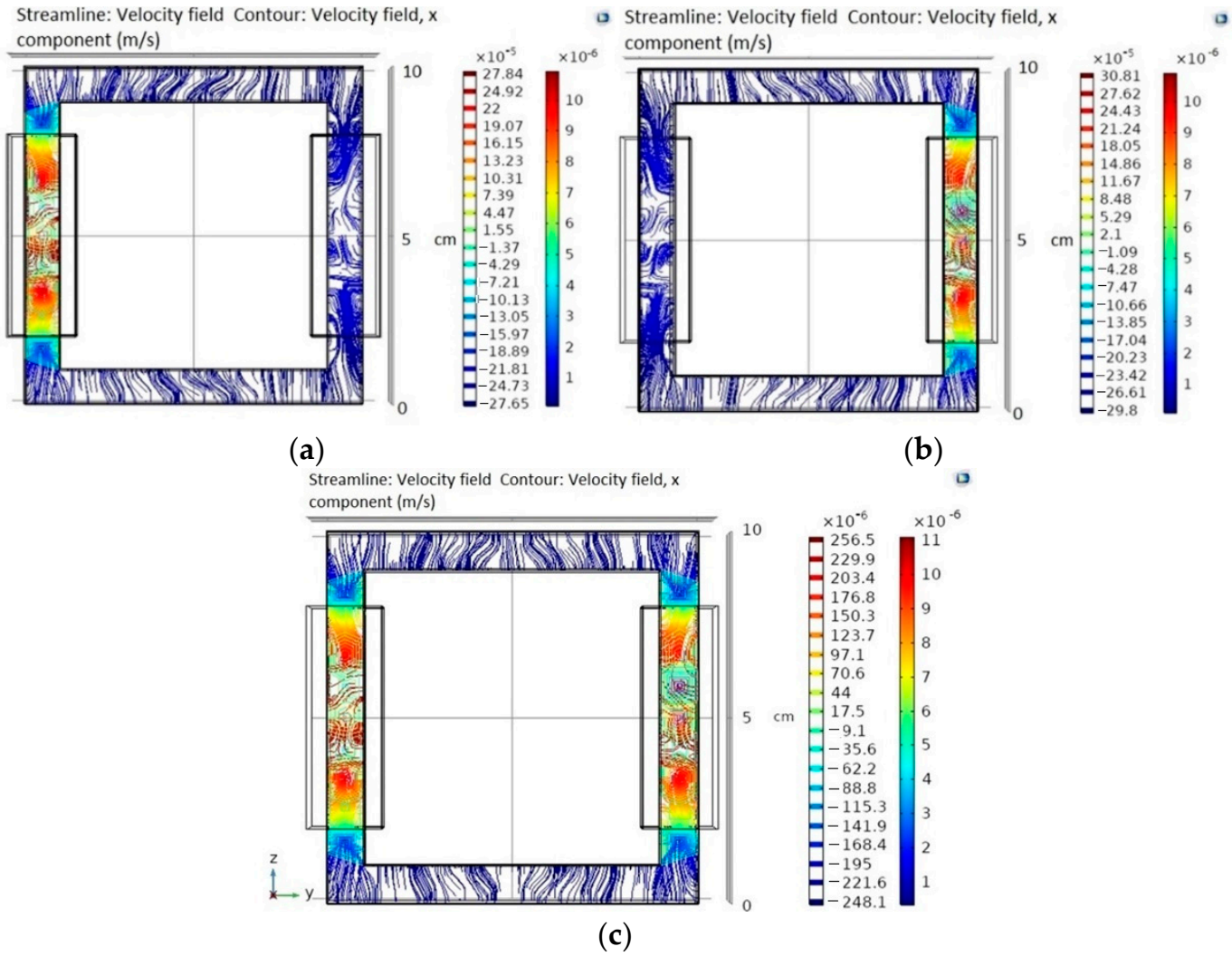

Figure 7. Stream tubes showing the velocity field patterns of the model: (**a**) Power is applied to the primary winding, (**b**) Power is applied to the secondary winding, (**c**) Power is applied to both windings excited by the same current.

According to Figure 9 it is obvious that the current excitation applied to primary winding for t = 0.14 ms, t = 0.15 ms and t = 0.16 ms leads to different values of flux density. Because the MFT is considered as a step-up transformer, an increment is observed in the flux lines of secondary winding side. The magnetic flux density component for x, y and z directions are indicated in Figure 10. The flux density has more quantities in z direction with comparison to y and z. This issue is directly dependent on the geometry defined for the transformer.

The parameters and descriptions defined for designed transformer are given in Table 3.

In order to obtain the relationship between simulation parameters and the output characteristics of the model, the second phase of the simulation study is processed. In this phase, all parameters but the dispersed phase concentration φ_d are the same as the previous study. Following the simulation steps, the *B-H* curves for various concentrations of dispersed phase φ_d in the same carrier are evaluated and plotted in Figure 11. The concentration rate has a percentage quantity between 10% and 90%. As the percentage raises, the saturation magnetization increases for the same amount of magnetic flux intensities applied.

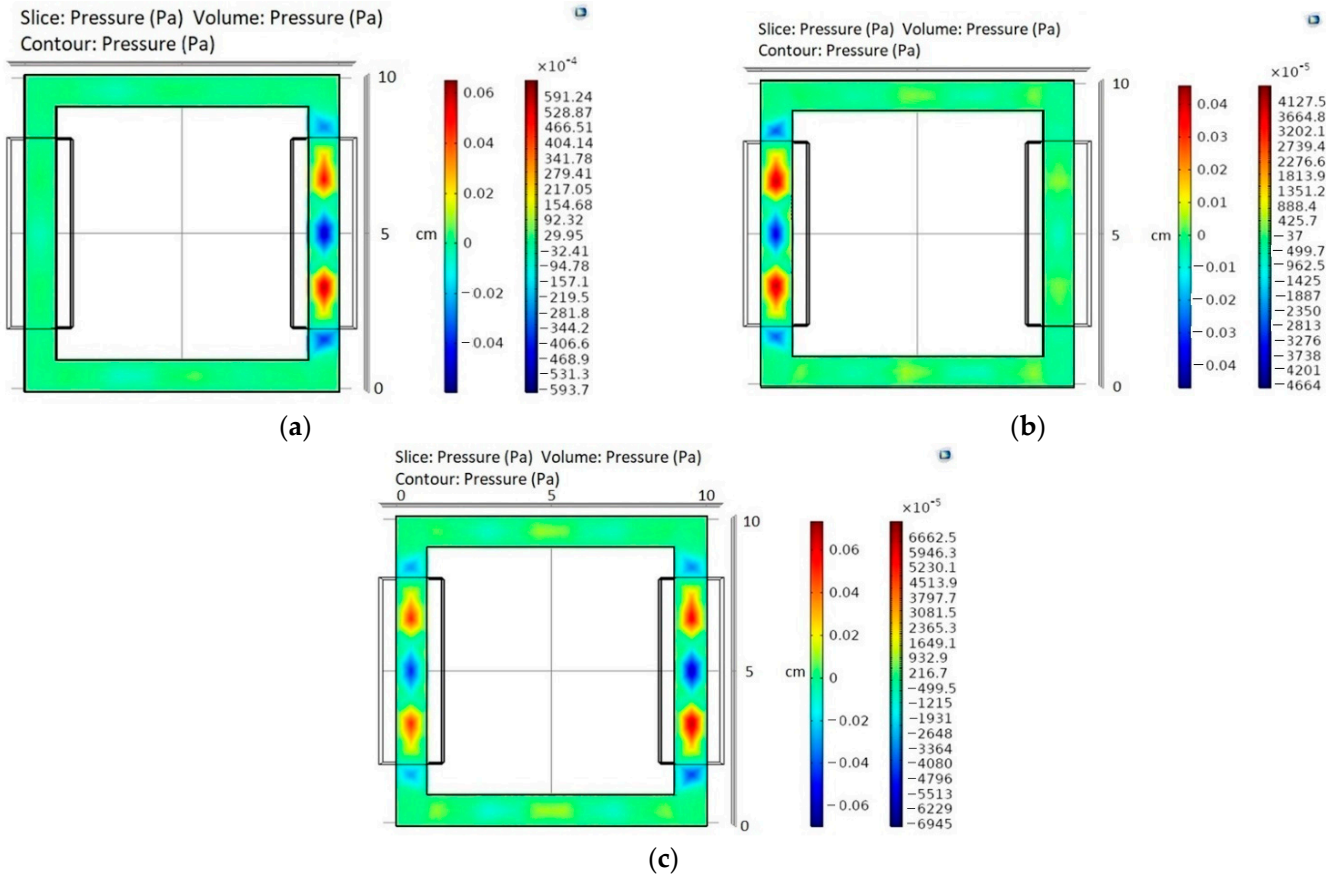

Figure 8. Pressure patterns for different powering schemes of the model: (**a**) Power is applied to the primary winding, (**b**) Power is applied to the secondary winding, (**c**) Power is applied to both windings excited by the same current.

It is important to notice that these evaluations and plots are enhanced for a special operating frequency of MFT operation. Hence, it can be concluded that the secondary winding voltages exhibit different behavior with respect to frequency and primary winding voltage. The waveforms of the secondary winding voltage by raising the iron powder mass concentration for the case when a 4 Ω resistor is connected to the secondary winding are presented in Figure 12. The optimum power obtained from the secondary windings is also an important issue due to the impedance matching. While the results of Figure 13a are higher than the ones in Figure 13b, we can conclude that the electrical load R = 0.3 Ω is matched by the impedance of transformer.

According to simulation results, the output voltage and power rise with respect to increased magnetic particles mass fraction for 5 *V* peak-to-peak input voltage applied to primary winding. However, the voltage amplitude decays, when the magnetic particle mass is increased further as depicted in Figure 14. The existence of an optimum magnetic particle mass fraction, which results in the maximum flux variation over time for the core and is solely reliant on the iron powder ratio, is demonstrated by this fact. In other words, by increasing the magnetic property of the liquid, the core's magnetic properties are enhanced.

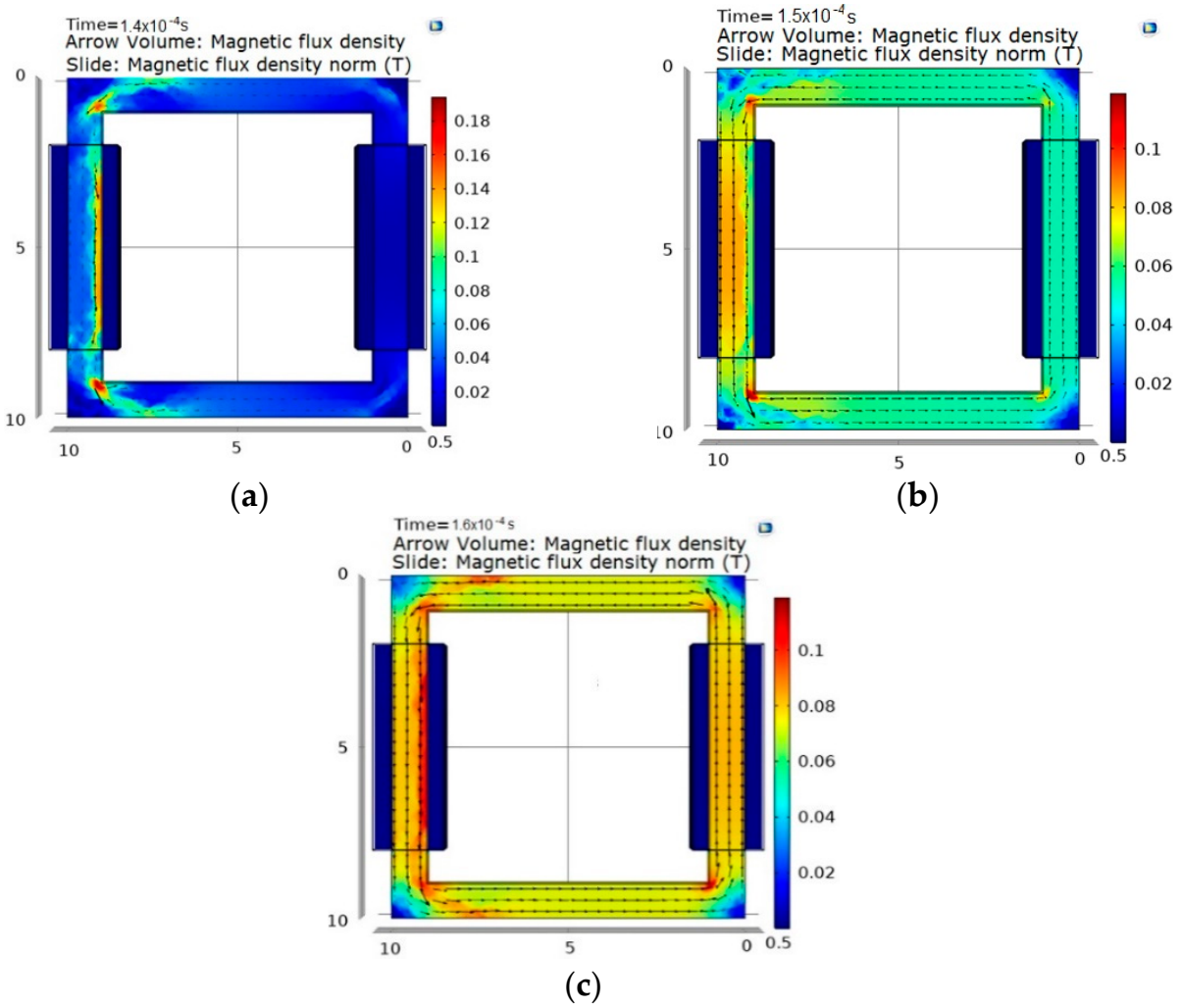

Figure 9. The magnetic flux densities and the flowing flux for (**a**) t = 0.14 ms, (**b**) t = 0.15 ms, (**c**) t = 0.16 ms.

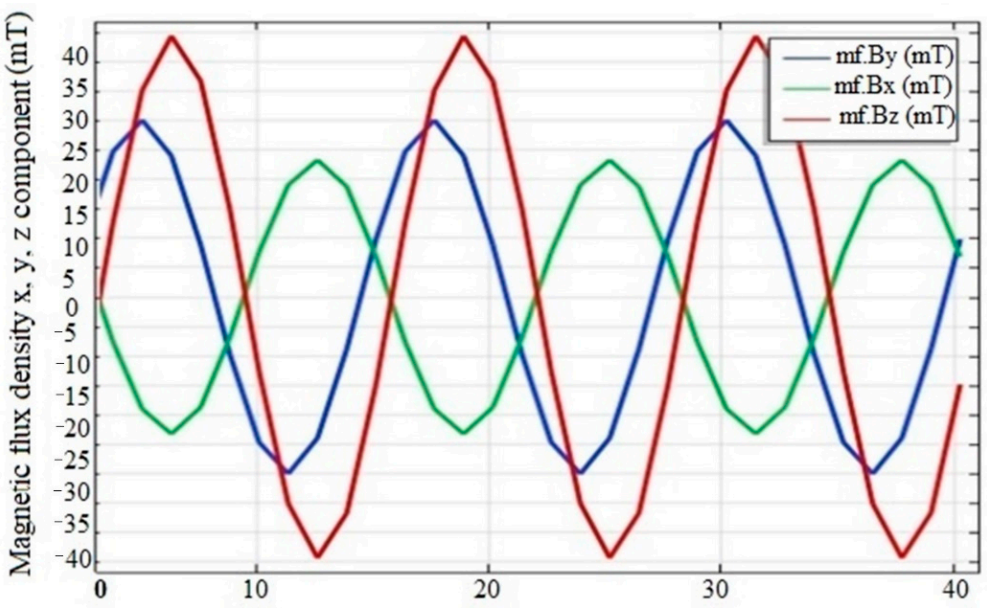

Figure 10. The generated magnetic flux density components.

Table 3. The MFT parameters and descriptions.

Parameter	Description
Core geometry (x) (cm)	10
Core geometry (y) (cm)	10
Core geometry (z) (cm)	1
Primary winding	10
Secondary winding	80
Coil type	Square
Coil wire conductivity (S/m)	(60) (10^7)
Conductor model	Homogenized multi-turn
Coil wire cross section area (m^2)	10^{-6}
Coil excitation	5 V

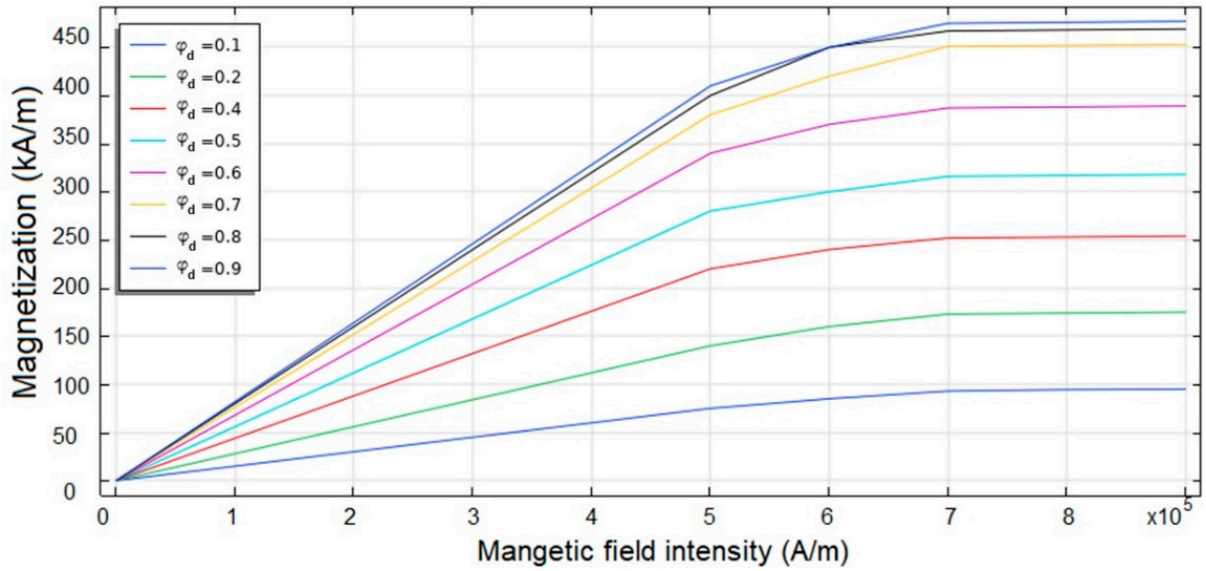

Figure 11. The magnetization curve generated for various concentration rates of the magnetic fluid.

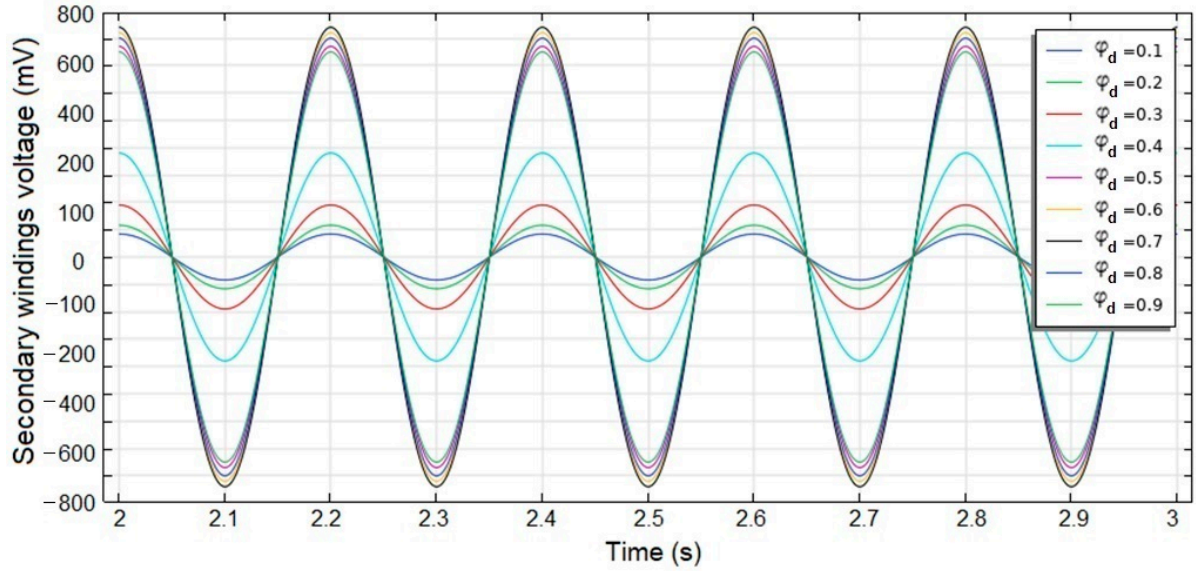

Figure 12. The secondary winding voltage waveforms for various dispersed phase mass fraction of the magnetic fluid.

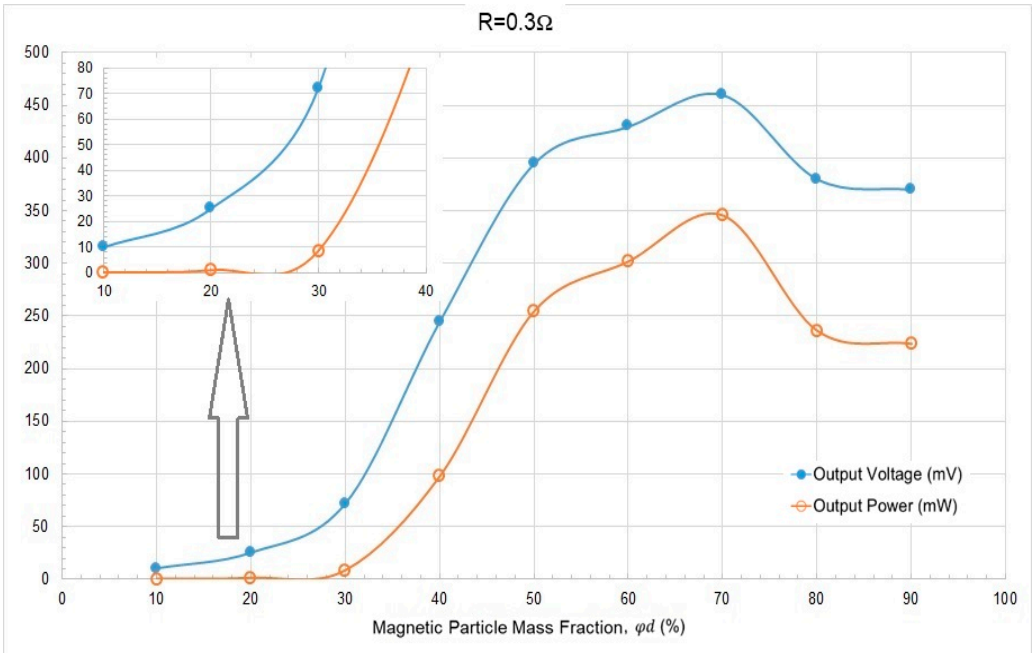

(**a**)

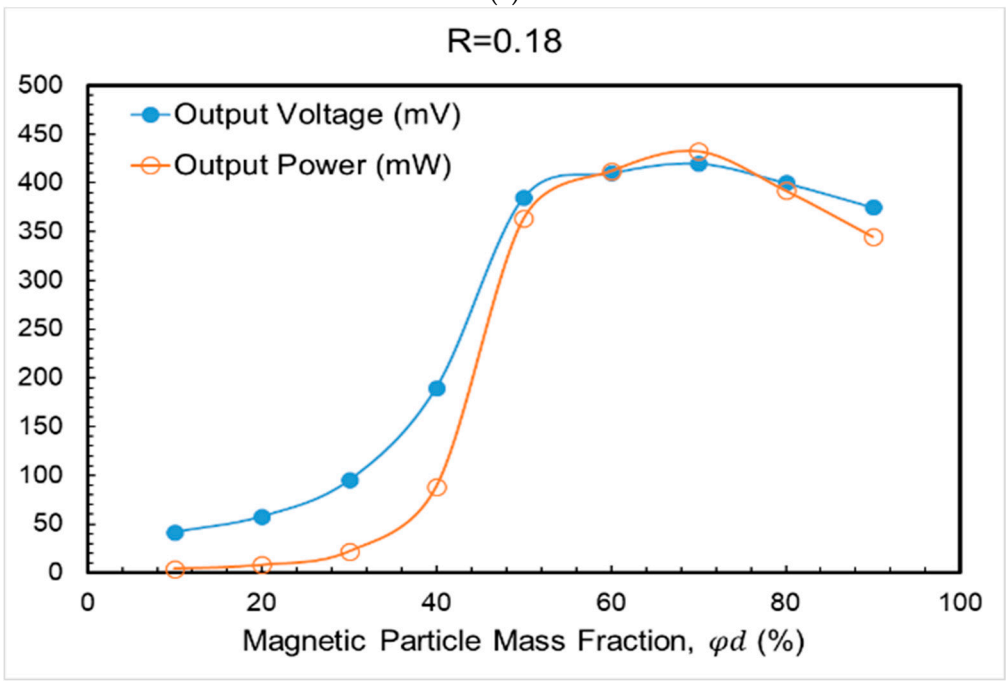

(**b**)

Figure 13. The secondary winding voltage and power for various mass fraction of magnetic particles in the magnetic fluid. The electrical loads of secondary windings are (**a**) R = 0.3 Ω and (**b**) R = 0.18 Ω, respectively.

It is obvious that the output voltage and power increase with respect to increasing load, although after reaching the maximum frequency rage (around f = 12 MHz) the output voltage and hence the output power starts to decay. The maximum output power is obtained for R = 3.2 Ω. Consequently, the operating characteristics (i.e., output voltage and power) of the MFT vary particularly well in 9–13 MHz frequency range while adding various loads to secondary side as they are depicted in Figures 14 and 15, respectively. The major advantage of changing the magnetic property by raising the magnetite concentration inside the fluid is that there is no permanent magnetization in the hysteresis of the magnetic

fluids. The disadvantage is the increase in the magnetic particle concentration and the increase in energy losses in the core at high frequencies (i.e., MHz). However, the effect of this increase on the output characteristics of the transformer in weak power transformers should be examined and evaluated separately. In addition, different doses of magnetic nanoparticles in carrier fluid also change the classical meaning of these fluids.

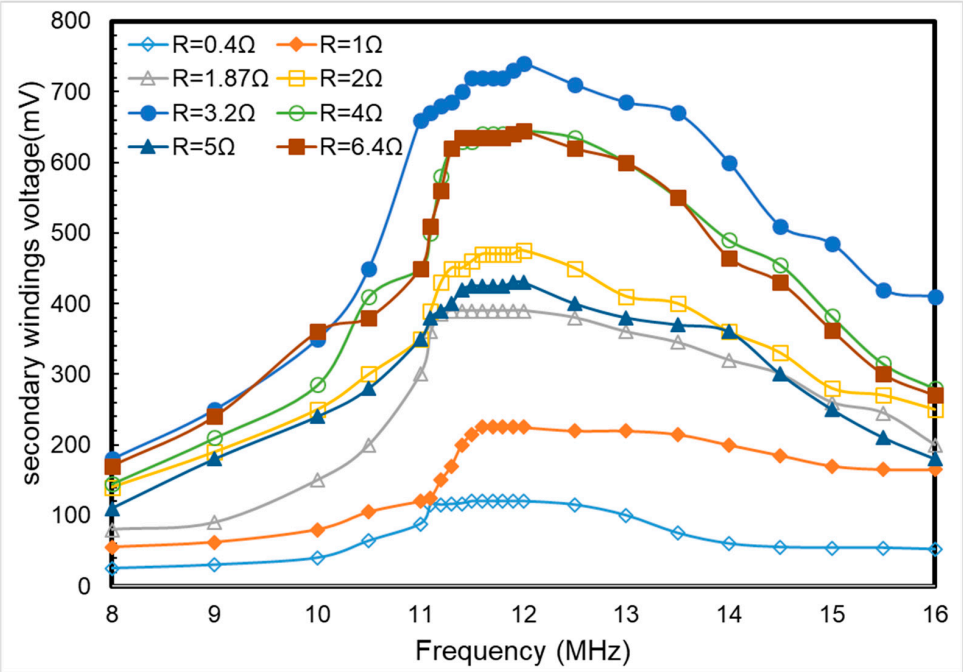

Figure 14. The output voltage characteristics with respect to frequency for various electrical loads attached to the secondary windings.

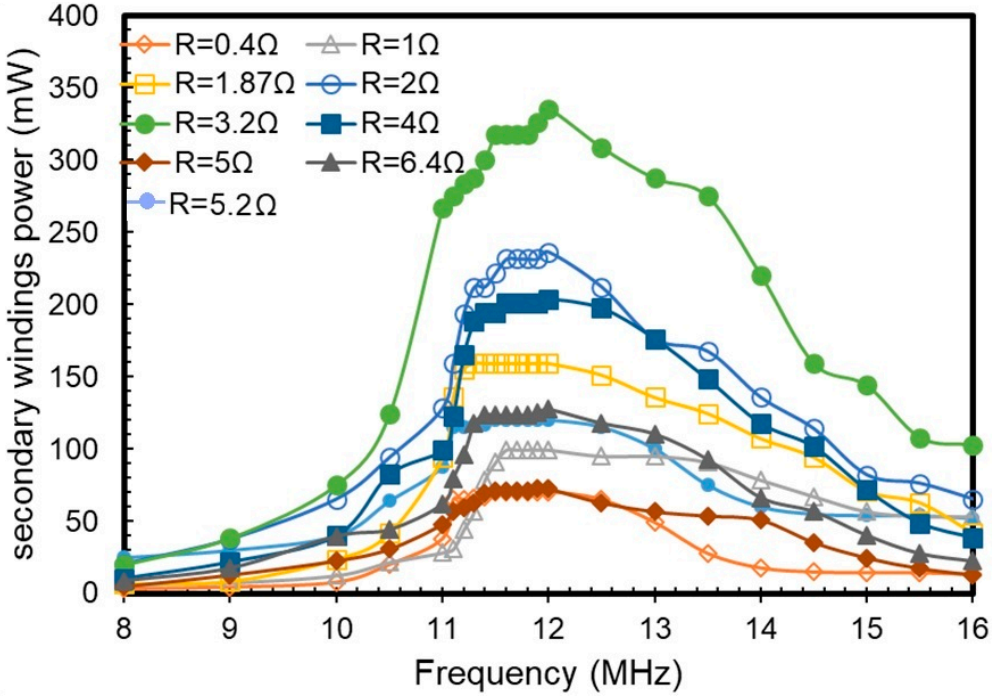

Figure 15. The output power characteristics with respect to frequency for various loads attached to the secondary windings.

4. Experimental Setup

Theoretical explanations, numerical calculations and simulation studies of the magnetic fluid core transformer have been emphasized in previous sections. This section considers the application of the magnetic fluid core transformer. The preparation procedure, characterization of structural, magnetic and electrical properties are presented for each step. The materials required for system design are prepared and the structural studies of the system are presented. The materials properties used for the experimental study are compiled in Table 4.

Table 4. The materials used in experimental studies and their properties.

Material	Description
ferromagnetic particle	Iron powder (d = 70 μm)
Insulating base	Engine oil (ρ = 874 kg/m^3)
Windings	Fine-stranded copper (d = 0.2 mm)
Primary windings No.	10
Secondary windings No.	80
Core size	10 cm × 10 cm × 1 cm
Core mold	Thin plastic

In the experimental stage, the voltage signals with different frequencies produced by a signal generator are applied to the primary windings of the transformer and the voltages produced in the secondary windings are observed. The signal generator used is Instek AFG-2125 type and has a wide frequency range from 1 kHz up to 25 MHz. Additionally, the optimal power generation based on different frequencies is determined using a variable electrical resistance table.

Figure 16 shows the prepared MFT samples and the windings wound on them. At first, 4 samples were prepared, and the experiments were conducted. Later, the 5th sample was obtained by adding iron powder to the sample with the densest mass fraction (yellow core), and the same experiments were repeated for this sample. For this reason, while the number of samples appears to be 4, in fact, a new structure was obtained by making changes in the last sample during the experimental stages. Thus, the variation of the output parameters with the change of the magnetic particle mass fraction was easily observed. Figure 17 shows the structure and image of the magnetic particles used in the sample cores. These particles consist of pure iron powder and have a diameter of 70 μm.

Figure 16. MFT samples with different magnetic particle mass fractions.

Figure 17. Structure of magnetic particles used in sample cores.

5. Experimental Results and Discussion

Experimental studies are conducted in two phases. In the first phase, the mass of iron powder in the liquid core is changed as the main parameter. Since it is possible to obtain maximum output power when the impedances are well-matched, the electrical load affecting the output power is taken into account as a parameter in the second phase. In the first step, tests are applied for unloaded condition and then testing results are conducted by connecting each sample to the same amount of load. The connections on the prototype are given in Figure 18 for the open circuit situation with different samples. The sinusoidal waveforms appear on secondary of MFT by applying 9.9 volts to the primary windings. The most effective output is observed at 12 MHz frequency for all cases. Adjusting the mass densities of the magnetic particles was performed using the WF professional digital top precision weighing scale. The highest voltage is observed around 600mV for the yellow sample with magnetic particle mass fraction (φ_d) of almost 0.6–0.8.

According to revealed oscilloscope images, the output characteristic of the transformer varies with respect to the magnetic particle mass fractions. Similar to simulation study, as the mass fraction increases, the magnetic properties of the general structure and thus the output voltages increase. While the decrease occurs after φ_d = 0.8 in the simulation studies, the output values decrease around φ_d = 0.6–0.8 and the exact decreasing point is not currently reachable due to measurement precision and probable error that occur in the experimental environment.

The output voltage and power levels are obtained by connecting a resistor table to the secondary windings of MFT samples as presented in Figure 19. The output voltage waveforms for various loads are given in Figure 20. As following the process, Figures 21–25 represent the voltage and power graphs obtained with different magnetic particle mass fractions for R = 0.15 Ω, R = 0.18 Ω, R = 0.2 Ω, R = 0.22 Ω and R = 0.3 Ω, respectively.

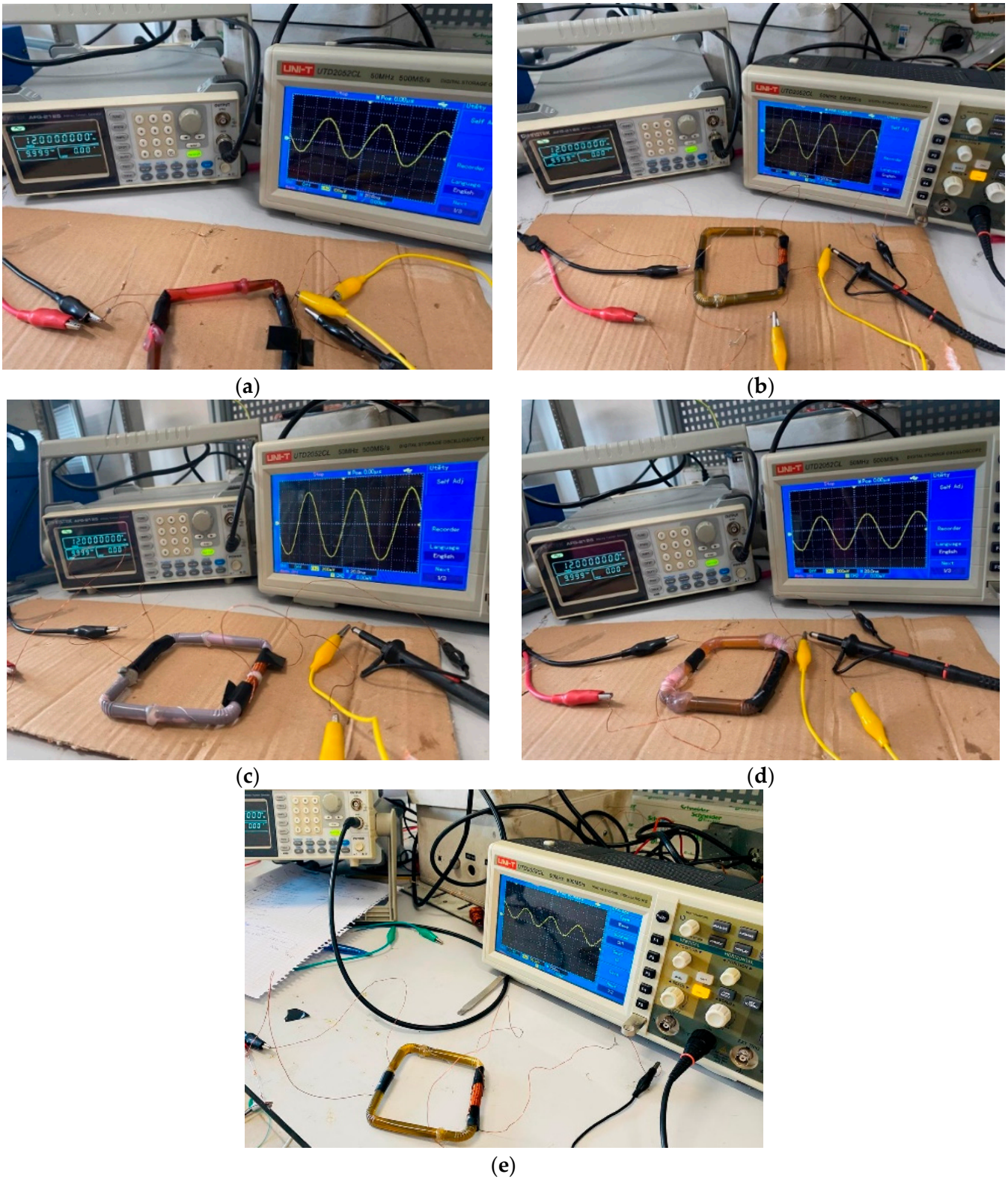

Figure 18. Open circuit tests for samples of different mass fractions made of ferromagnetic particles and engine oil (**a**) with φ_d = 0.2–0.3, (**b**) with φ_d = 0.3–0.4, (**c**) with φ_d = 0.4–0.6, (**d**) with φ_d = 0.6–0.8 (**e**) with φ_d >0.8.

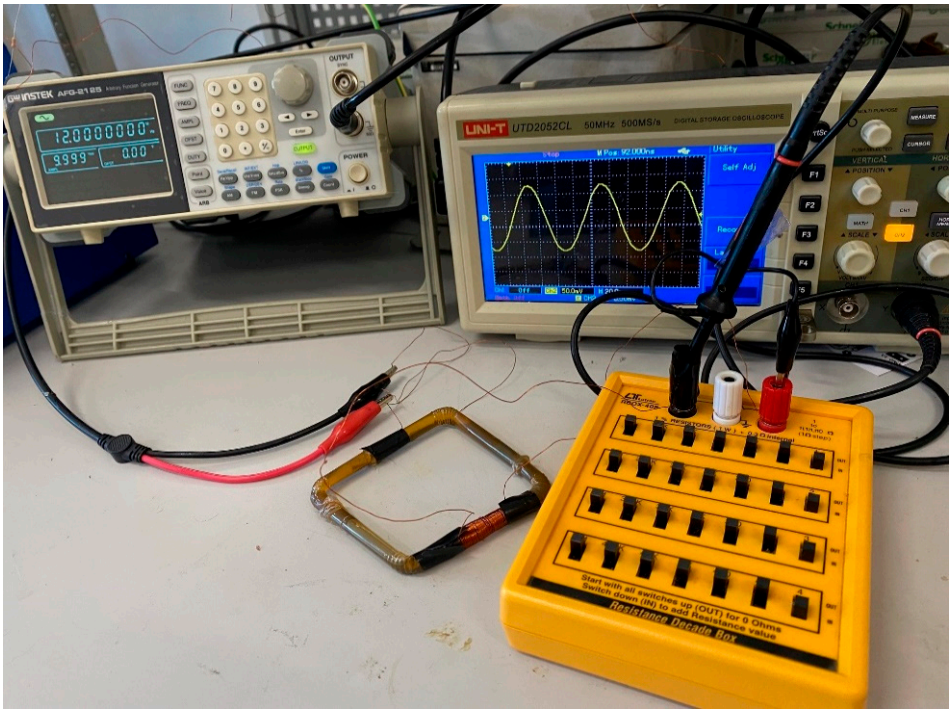

Figure 19. MFT sample connected to the resistor table in order to visualize the output for various resistors.

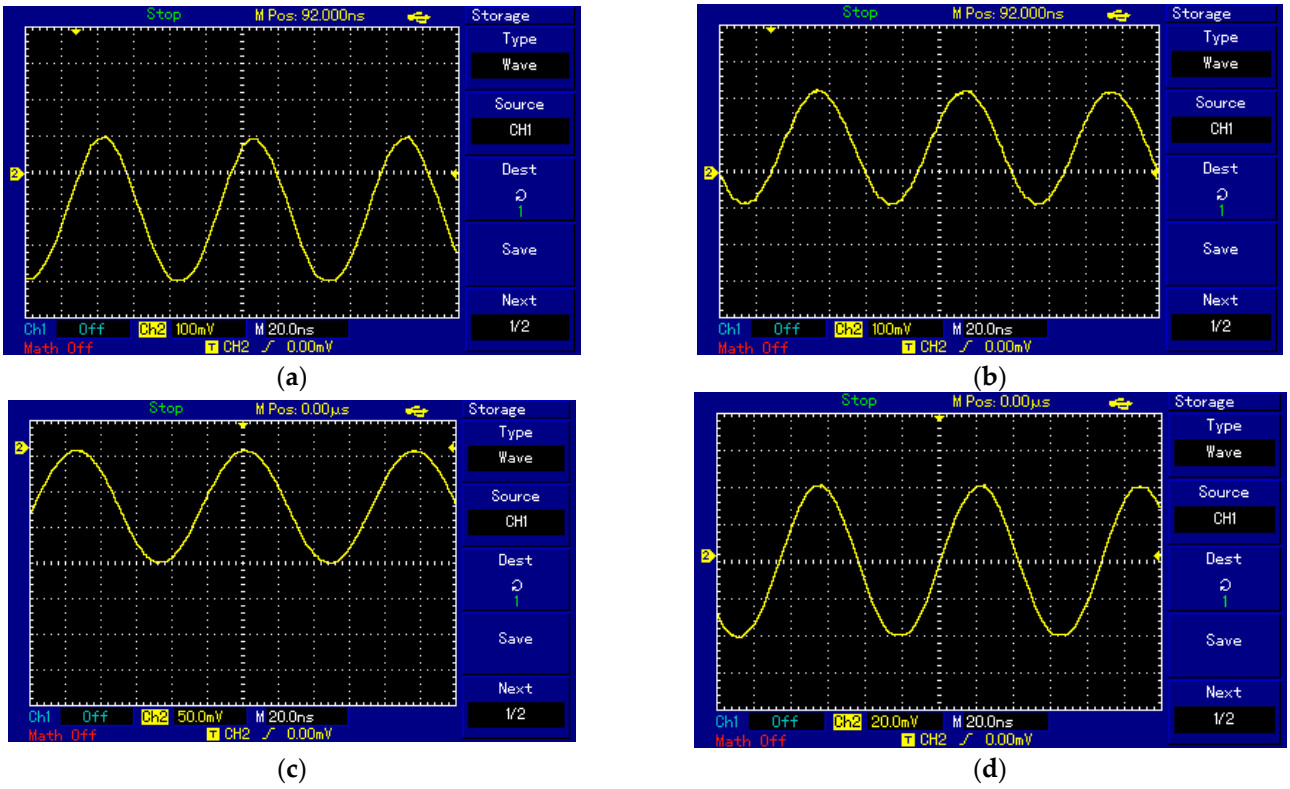

Figure 20. MFT output voltages waveforms for (**a**) R = 0.2 Ω (**b**) R = 1.87 Ω (**c**) R = 1 Ω and (**d**) R = 0.4 Ω.

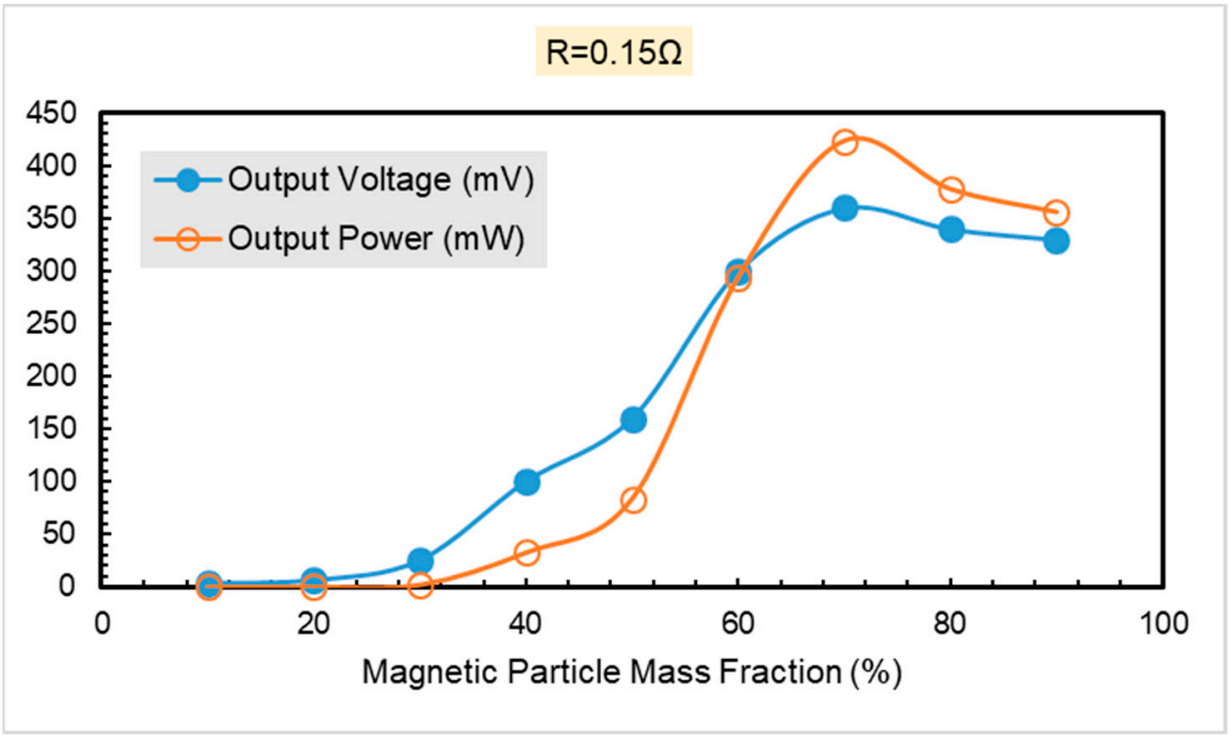

Figure 21. Voltage and power data with various magnetic particle mass fraction for R = 0.15 Ω.

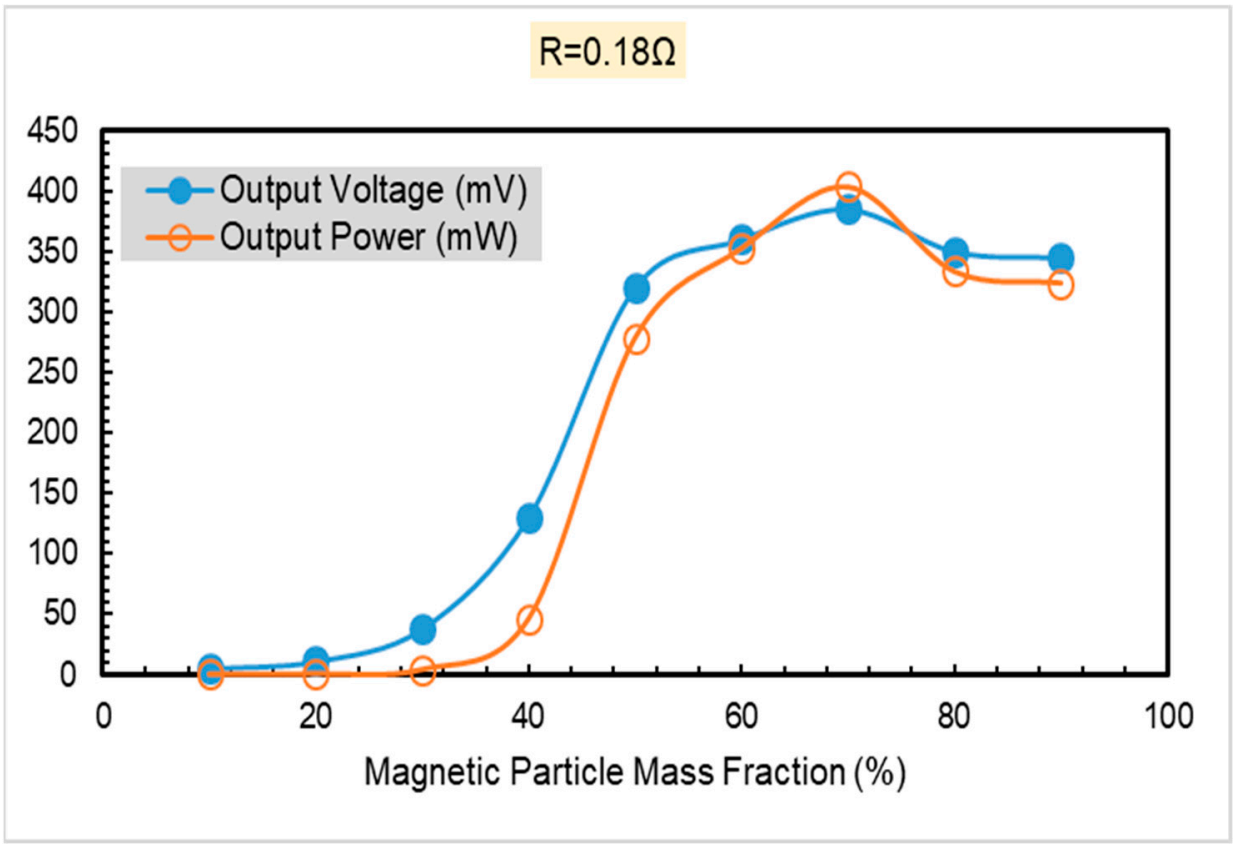

Figure 22. Voltage and power data with various magnetic particle mass fraction for R = 0.18 Ω.

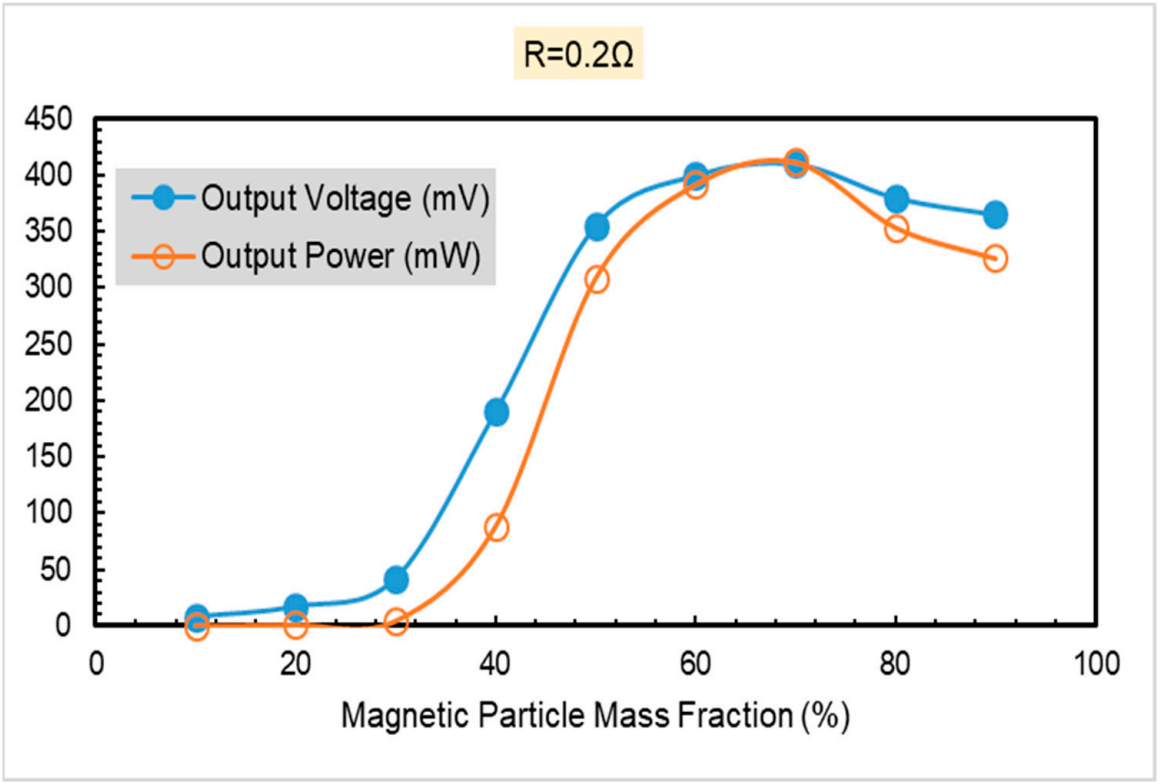

Figure 23. Voltage and power data with various magnetic particle mass fraction for R = 0.2 Ω.

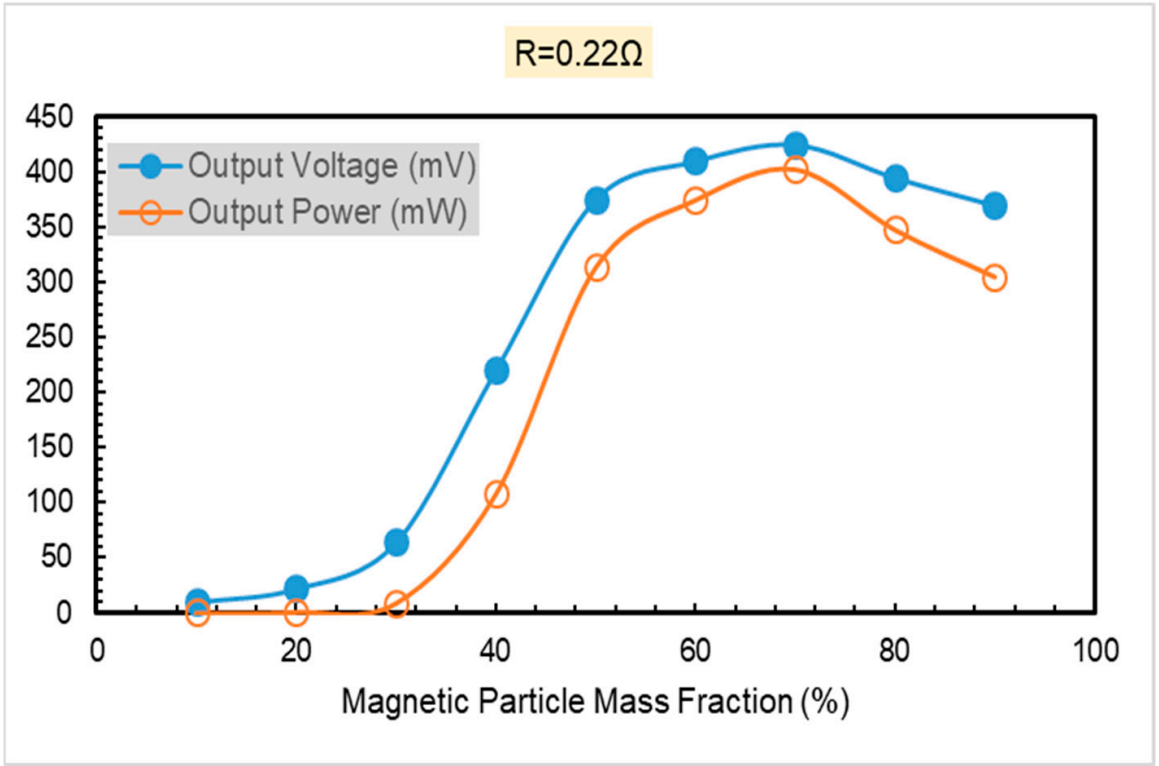

Figure 24. Voltage and power data with various magnetic particle mass fraction for R = 0.22 Ω.

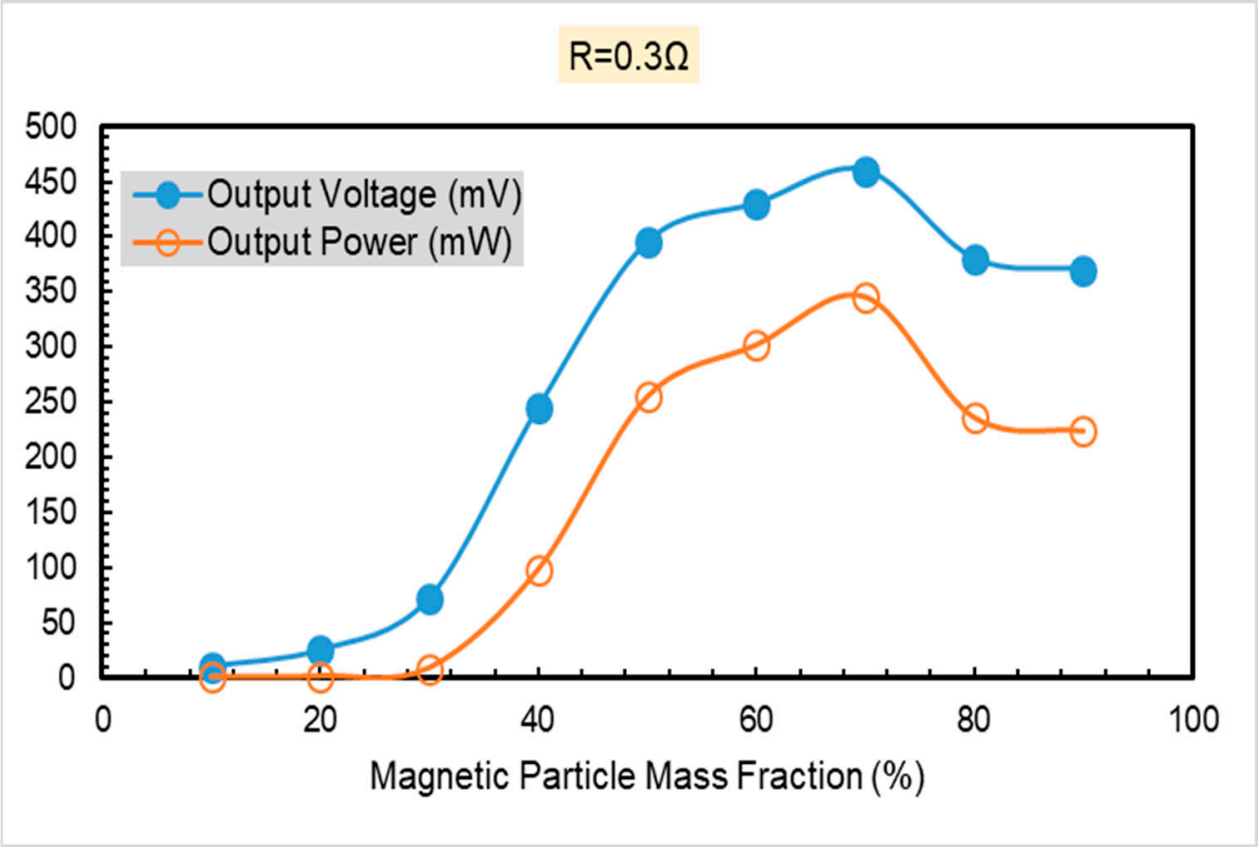

Figure 25. Voltage and power data with various magnetic particle mass fraction for R = 0.3 Ω.

According to the obtained results, the magnetic mass fraction fluctuates up to φ_d = 0.6. This applies to all existing loads. For the loads below R = 0.2 Ω, the power and the voltage graphs overlap, and the power level rises above the voltage level in a certain range. However, this is not valid for loads larger than 0.2 Ω and the output voltage is always above the output power.

In the second phase of the experimental studies, the electrical load affecting the output power at different frequencies was taken into account as the key parameter. In this direction, the output characteristics of the fluid core transformer were investigated with frequency variation by connecting different loads to the secondary windings of a single sample. As the final step, by graphing the data obtained from the experimental study with different loads, the MFT output voltage and power at different frequencies are plotted. Figures 26 and 27 indicate the output voltage and power data for R = 0.4 Ω, R = 1 Ω, R = 1.87 Ω, R = 3.2 Ω, R = 4 Ω, R = 5 Ω and R = 6.4 Ω.

Considering the output voltage graph of the MFT with different loads, it is observed that the highest voltage value is obtained when R = 3.2 Ω. For all loads, the voltage level offers the highest value in the f = 11 MHz to f = 13.5 MHz range (V = 526 mV). Considering the output power graph of the transformer designed in the same way with different loads, it exhibits the most efficient behavior in terms of system output power in the frequency ranges f = 11.2 MHz and f = 13 MHz. Here again, the highest power value is obtained for R = 3.2 Ω and R = 1.87 Ω in the secondary winding (P = 188.8 mW).

In accordance with the experimental tests, as the results obtained are compared with the simulation studies, although the output data differ to a certain extent, the transformers designed in the same frequency ranges in both cases exhibit similar characteristics and behavior. The proof of this situation is conducted by comparing the results obtained from both studies. In Figures 28–30, the output voltages obtained from the simulation program and experimental studies for R = 0.4 Ω, R = 3.2 Ω and R = 6.4 Ω, in the same frequency ranges are presented.

According to obtained data, an almost equal difference is observed for all three load cases ($\Delta V \approx 200$ mV). This value, which occurs at the output voltage level, may be caused by different reasons. The most obvious of these reasons is the measurement errors that can occur when adjusting and measuring the mass of magnetic particles. Another reason is the accretion action of magnetic particles in the carrier base due to their masses. Particles collected in a certain region of the transformer core weaken the magnetic flux formed in other regions and affect the output characteristics. However, since the dispersion method of magnetic particles is chosen homogeneously in the simulation program, this problem is completely eliminated, and the magnetic flux occurs proportionally and smoothly for all fractions. In the same way, the results obtained from the simulation studies and experimental findings are compared and the amount of power transferred to the secondary windings in both cases is shown. The output power obtained from the simulation program and experimental studies for R = 0.4 Ω, R = 3.2 Ω and R = 6.4 Ω for the same frequency ranges are presented in Figures 31–33.

According to literature, there are five leading works on the fluid cored transformers under different frequency regimes. They are summarized in Table 5 with the relevant features mentioned in corresponding papers. Note that all of them except [33] have complicated ferromagnetic fluid. The structure includes a cheap ferro-fluid, whereas its operation frequency is low compared to ours and other works if the work in Ref. [33] and the current one are compared. In one of our earlier works, namely Ref. [1], the issue has been analyzed only by simulation study and there is no practical and experimental study conducted in order to prove the precision of the application. In the designed transformer in [34], the output voltage of the transformer decreases rapidly at high frequencies. The main reason for the decrease in transformer efficiency at high frequencies yields to an increase in losses in magnetite (Fe_3O_4) particles contained in the magnetic fluid with frequency. In addition, the output characteristics of the transformer have a more stable structure in the range of 50–100 kHz and the maximum voltage obtained is about 46 volts. The coupling coefficient of inductors is increased with raising the frequency as the percentage of the dispersed phase is raised in [29]. However, there is no data about the efficiency of the transformer in terms of power and voltages. For the miniature planar spiral transformer with magnetic nanofluid core in [33], two types of magnetic nanofluid are used as core. By applying square wave form 10 $V_{p\text{-}p}$ voltage, the voltages for frequencies of 100 kHz, 300 kHz and 600 kHz are found as 2.6 V, 2.94 V and 3.4 V, respectively. The parameters belonging to the current research are given at the last row of Table 5. It is obvious that a comprehensive study has been conducted considering various loads with the aim of obtaining the optimum voltage and power ratings, while almost no research has focused on operating a magnetic fluid core transformer for mentioned ratings. The transformer proposed in the present work has higher frequencies compared to the one in Ref. [33] having a cheap fluid core.

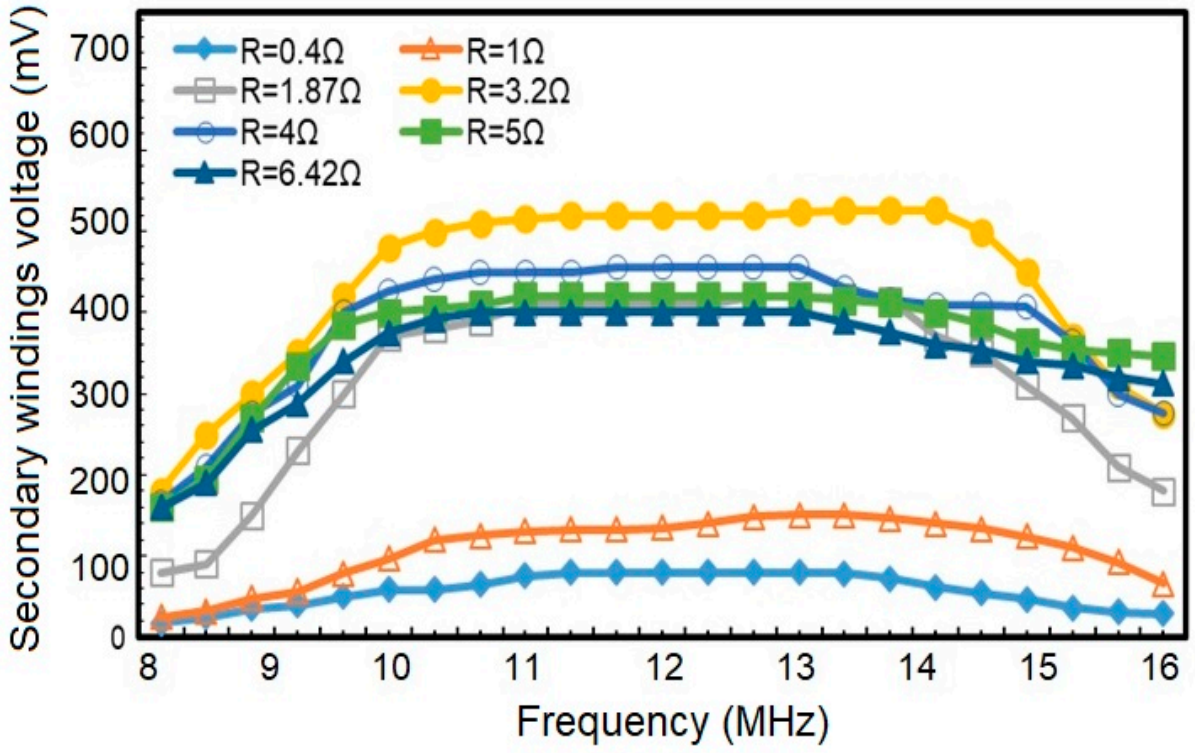

Figure 26. MFT output voltage with frequency variation with various loads.

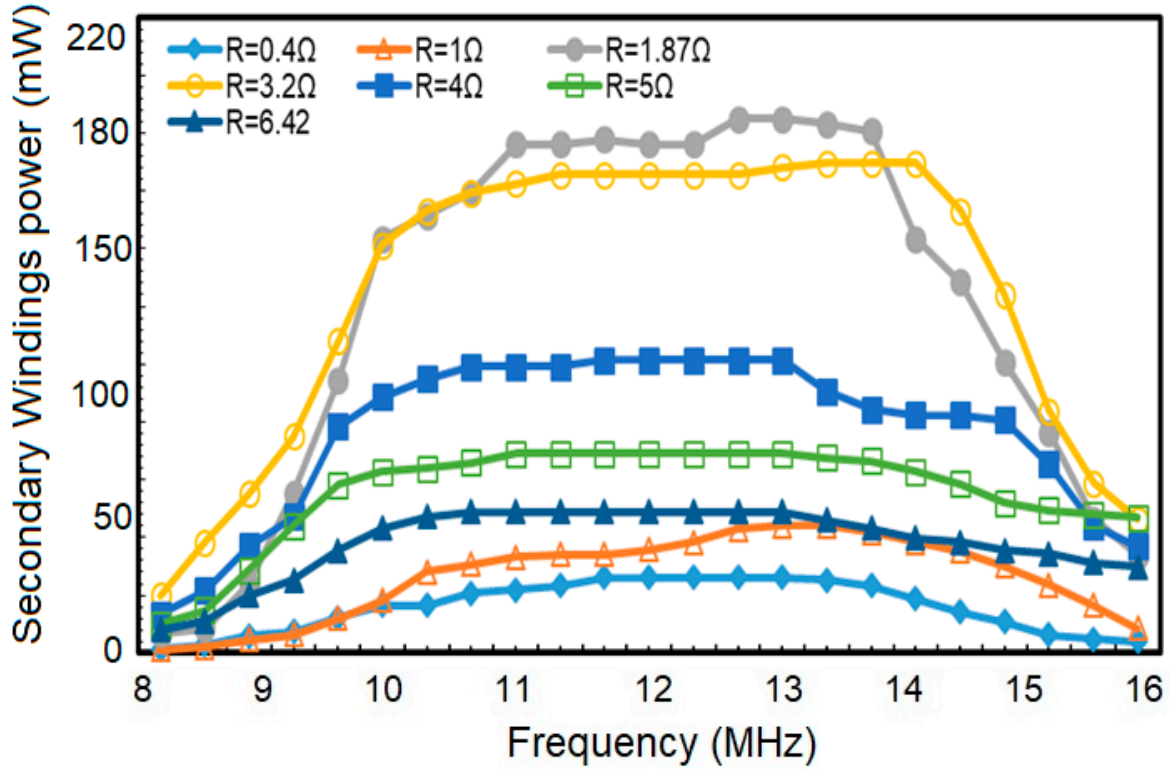

Figure 27. MFT output power with frequency variation with various loads.

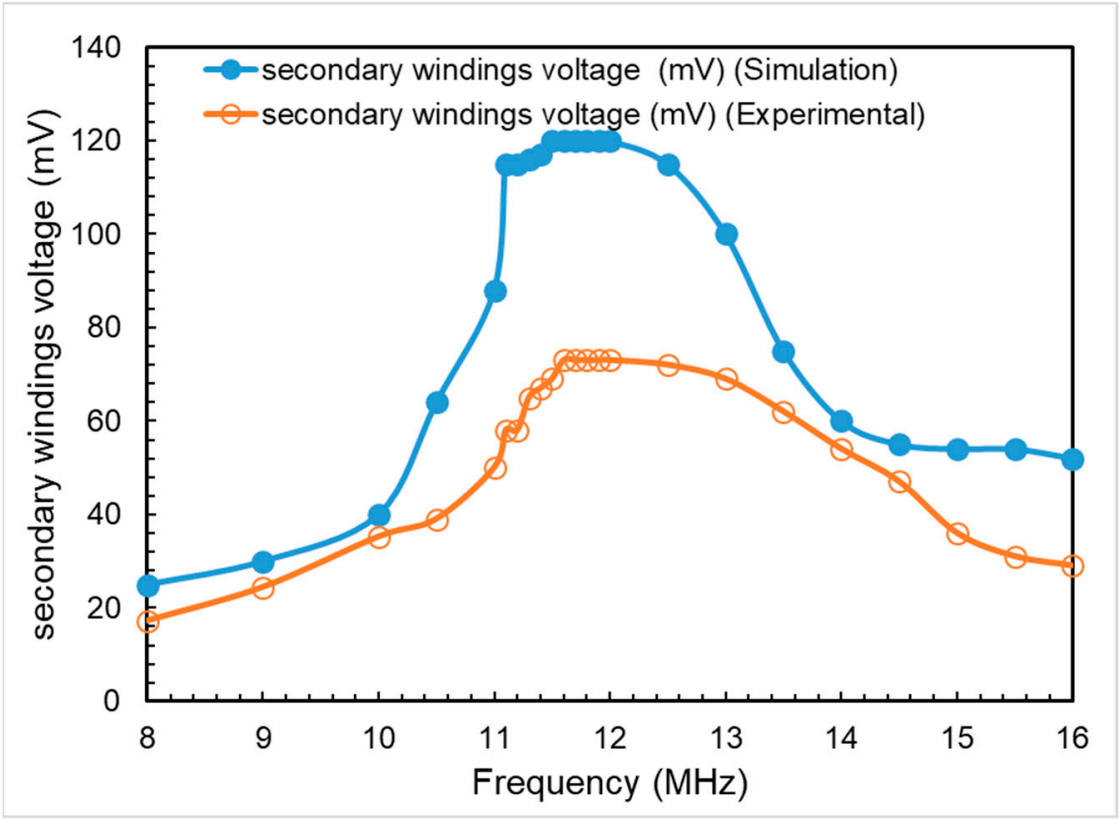

Figure 28. Output voltages acquired from simulation program and experimental studies for R = 0.4 Ω.

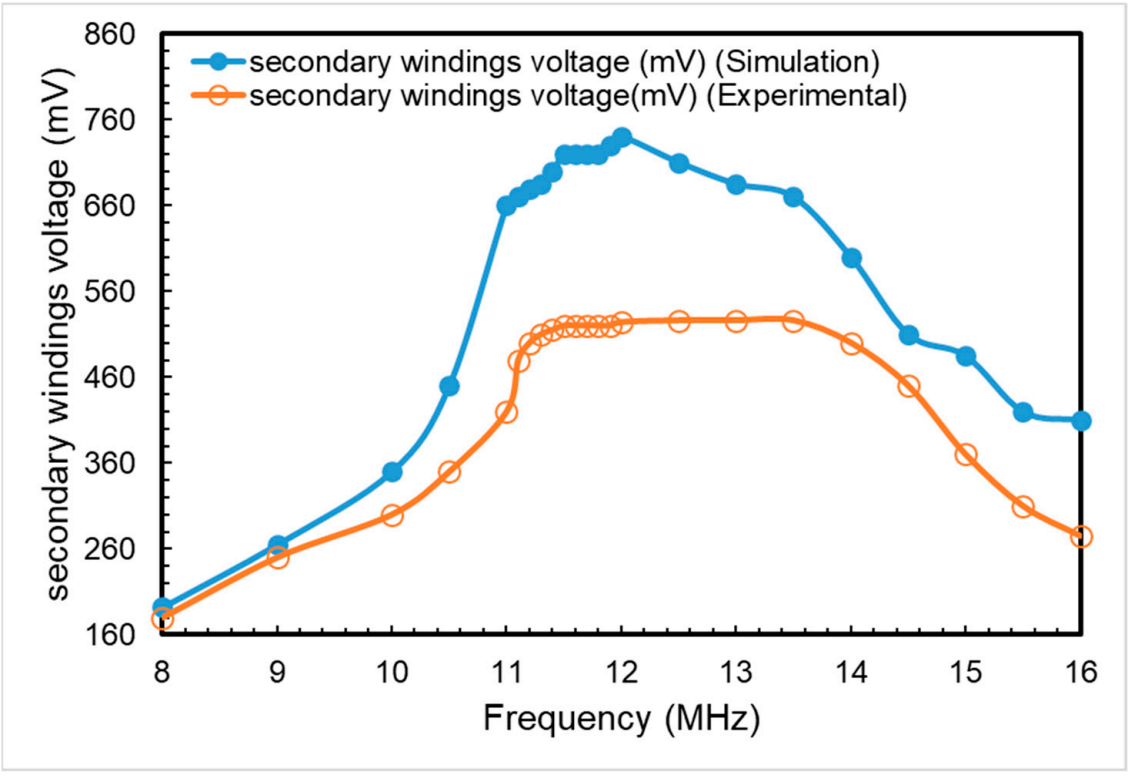

Figure 29. Output voltages acquired from simulation program and experimental studies for R = 3.2 Ω.

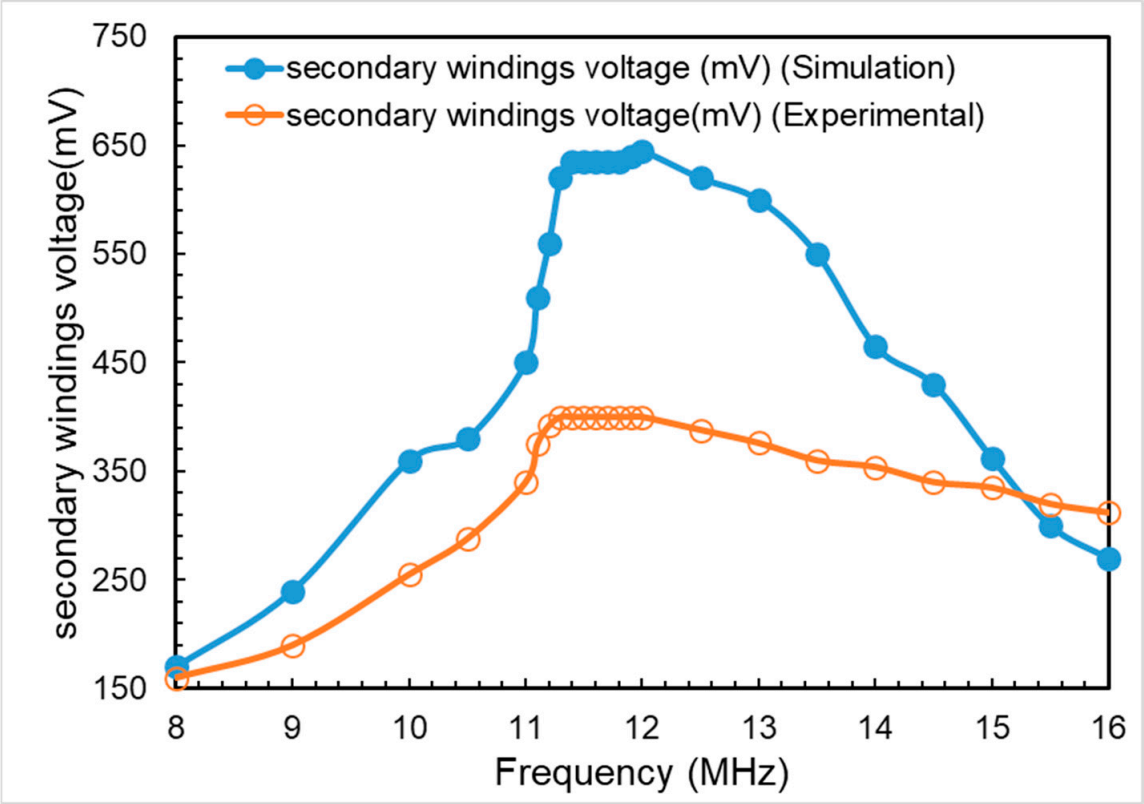

Figure 30. Output voltages acquired from simulation program and experimental studies for R = 6.4 Ω.

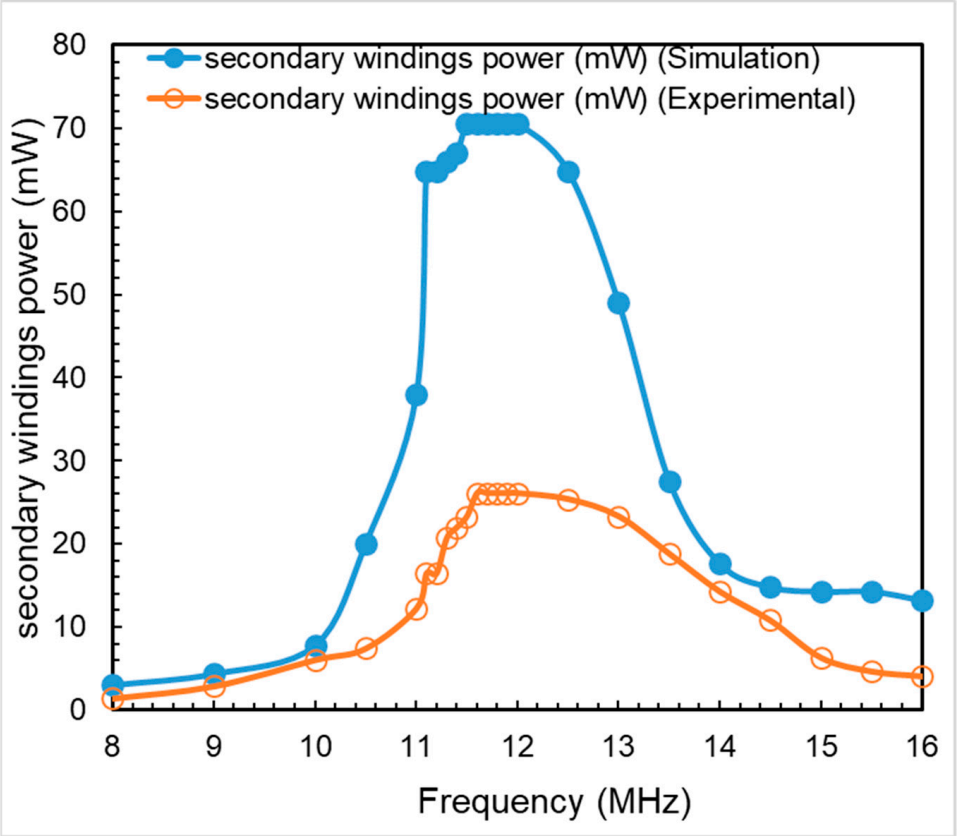

Figure 31. Output power acquired from simulation program and experimental studies for R = 0.4 Ω.

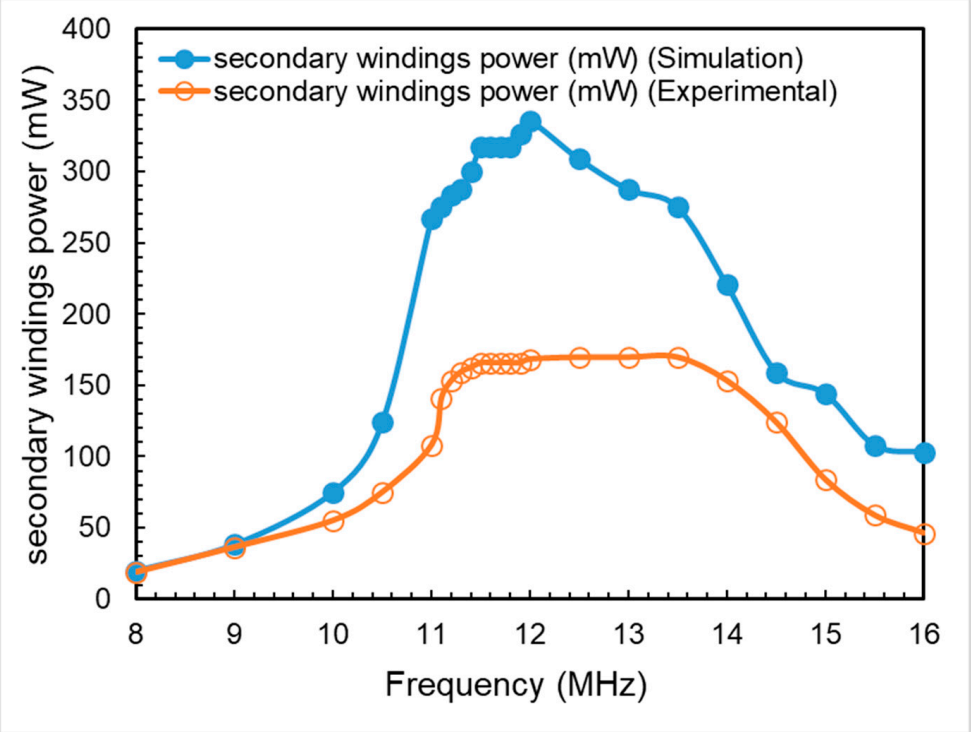

Figure 32. Output power acquired from simulation program and experimental studies for R = 3.2 Ω.

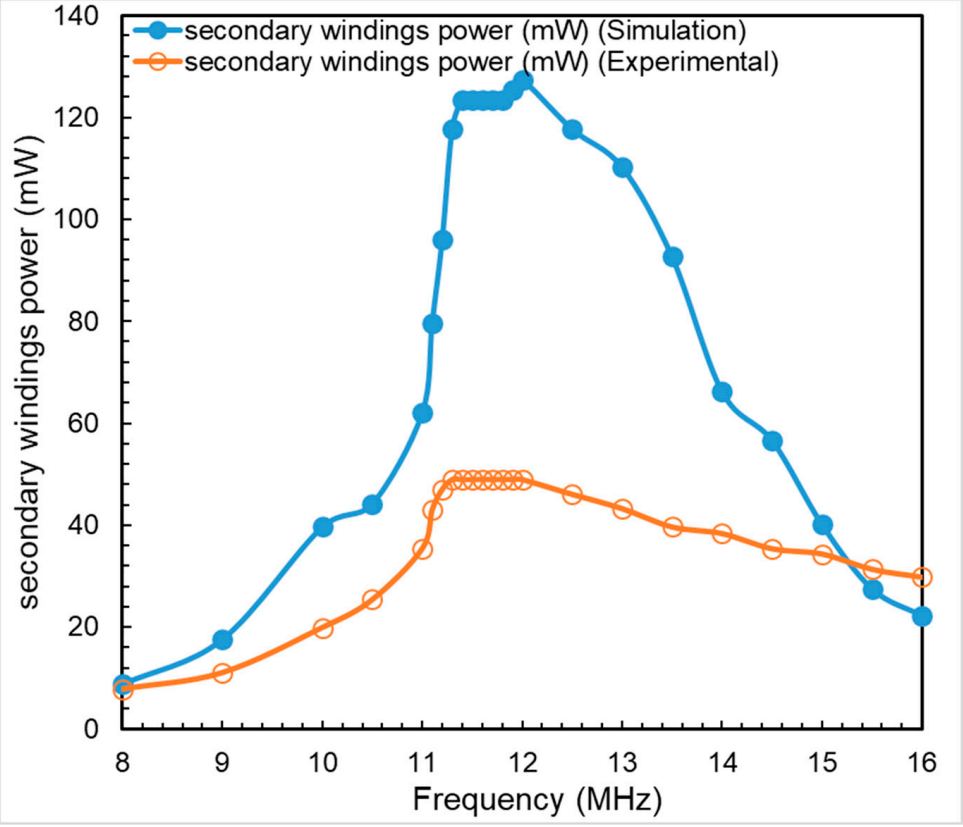

Figure 33. Output power acquired from simulation program and experimental studies for R = 6.4 Ω.

Table 5. Transformer applications of ferromagnetic fluids in different frequency ranges according to literature.

Material	Application	Trial Frequency	The Coupling Coefficient of Transformer Coils	Voltage Analysis	Power Analysis
Fe_3O_4, diesel oil, polydimethylsiloxane (PDMS) [29]	on-chip Micro-Transformer	100 kHz–100 MHz	15%	-	-
Chemical co-precipitation of Fe_3O_4, oleic acid, diesel oil [32]	Transformer	100 KHz–100 MHz	50%	-	-
100 Å (10 nm) magnetic nanoparticles dispersed in diesel oil [33]	Flow interactions in miniature Electric power transformer	50 Hz–1 KHz	-	-	-
DS-50 magnetic fluid, Fe_3O_4 [34]	Transformer	100 Hz–1 MHz	-	Maximum 3 V/46 V (100 kHz)	-
Magnetic Nanofluid UTR1000, Magnetic Nanofluid UTR500 [35]	Miniature Planar Spiral Transformer	100 KHz–600 KHz	High *Q* quality factors for both primary and secondary windings of MPST/MNF_500 MNF_500.	-	-
Iron powder (70 µm diameter), engine oil	Transformer	8–23 MHz	-	526 mV (12 MHz)	188.8 mW

6. Conclusions

The magnetic fluid core transformer (MFT) is suggested in this research as a way to lessen the eddy currents and core losses seen in traditional transformers. Magnetic fluid (ferrofluid) core carries the advantages of low conductivity ($\sigma = 1.5 \times 10^{-7}$ S/m) and super para-magnetism of oil-base magnetic fluidity simultaneously. The mathematical model and the numerical simulations of the transformer with windings are analyzed systematically. The study is concerned with different electric powering schemes providing the operational conditions considered and 3D models are used to compute the magnetic field, the magnetic fluid core flow and magnetic parameters of the MFT. The magnetic core is a stable, colloidal suspension of magnetic nanoparticles, dispersed in a fluid carrier with engine oil. The flowing physics type is turbulent and Wilcox k–ω model is used to solve them. The magnetic flux density formed at different particle densities is investigated and optimization studies are conducted on the simulation study until suitable values are obtained. Studies are presented in two phases. The first phase is conducted to obtain output power and voltage characteristics by connecting a single load and an open circuit experiment for various ferromagnetic particle fractions. The second phase is conducted to obtain output power and voltage characteristics by connecting different loads to the secondary windings of the same sample with a mass fraction of magnetic particles at high frequency. According to the simulation results, with varying the applied frequencies, the most stable frequency range where the MFT operates, is 11–13 MHz. The density of ferromagnetic particles also affects these values. The highest output voltage and power values are obtained at the density of 60% to 70% ferromagnetic particles. For lower and higher values of mass fraction, voltage and power at the secondary windings are varied. It has been observed that the electrical properties and output power and voltage characteristics of the designed transformer in the prototype environment are similar to those of industrially used transformers at high frequency values. Thus, in the frame of the present results, instead of using expensive magnetic fluids, cheap and efficient magnetic fluid cores can be replaced for several manufacturing purposes. Future works include the determination of experimental analysis for MFT by examining several magnetic nanoparticle-oil suspensions with the distinct concentration of magnetic nanoparticles in the base fluid, in order to enhance the best operating results in terms of magnetic flux density production, obtaining the optimal magnetic body forces, and hence attaining the best magnetization level of MFT. In addition, evaluation of the core losses and generally the overall power losses occurring in high frequency transformers is an essential demand as a novel perspective

for strengthening utilization of the proposed and designed system. The maximum power and voltage from the secondary windings are found as 526 mV and 188.8 mW for the experimental studies.

Author Contributions: Conceptualization, E.K. and S.H.; methodology, E.K.; software, E.K. and S.H.; validation, E.K.; formal analysis, S.H.; investigation, E.K., S.H.; resources, E.K.; data curation, S.H.; writing—original draft preparation, E.K. and S.H.; writing—review and editing, E.K. and S.H.; visualization, S.H.; supervision, E.K.; project administration, E.K.; funding acquisition, E.K. All authors have read and agreed to the published version of the manuscript.

Funding: This research received no external funding.

Institutional Review Board Statement: Not applicable.

Informed Consent Statement: Not applicable.

Data Availability Statement: Not applicable.

Conflicts of Interest: Authors declare no conflict of interest.

References

1. Hatem, S.; Kurt, E. The simulation of a new high frequency transformer. *J. Energy Syst.* **2022**, *6*, 322–337. [CrossRef]
2. Kul, S.; Iskender, I.; Balci, S. FEA Simulation of the Electromagnetic Effects on the Flux Distribution of the Joints in the Transformer Core Structure. In Proceedings of the ISMSIT 2018 2nd International Symposium on Multidisciplinary Studies and Innovative Technologies, Ankara, Turkey, 19–21 October 2018; pp. 1–5. [CrossRef]
3. Isa, M.Z.; Kadir, A.; Gomes, C.; Azis, N.; Izadi, M.; Alyozbaky, O.S.H. Analysis on magnetic flux density and core loss for hexagonal and butt-lap core joint transformers. In Proceedings of the SPEC 2016 IEEE 2nd Annual Southern Power Electronics Conference, Auckland, New Zealand, 5–8 December 2016; pp. 1–4.
4. Tomczuk, B.; Koteras, D. Magnetic flux distribution in the amorphous modular transformers. *J. Magn. Magn. Mater.* **2011**, *323*, 1611–1615. [CrossRef]
5. Aina HAnding, W.; Shiqiang, Y. Dynamic magnetic characteristics of Fe78Si13B9 amorphous alloy subjected to operating temperature. *J. Magn. Magn. Mater.* **2016**, *408*, 159–163.
6. Ahmad, M.K.; Ali, M.S.; Majid, A.; Saleem, J.; Kazmi, S.M.R. Comparison and analysis of core materials for high frequency (1MHz) planar transformers. In Proceedings of the 2018 International Conference on Computing, Mathematics and Engineering Technologies (iCoMET), Sukkur, Pakistan, 3–4 March 2018; pp. 1–5.
7. Goo, J.; Kim, Y.; Lee, S.; Kim, W.; Lee, J.; Choi, K. Magnetization Loss Estimation of HTS Solenoid Coils Wound With CORC. *IEEE Trans. Appl. Supercond.* **2020**, *30*, 1–7. [CrossRef]
8. Mogorovic, M.; Dujic, D. Modeling and Experimental Verification of Geometry Effects on Core Losses. In Proceedings of the 10th International Conference on Power Electronics and ECCE Asia (ICPE 2019—ECCE Asia), Busan, Republic of Korea, 27–30 May 2019; pp. 3040–3046.
9. Wojtkun, J.; Bródka, B.; Stachowiak, D. The influence of core geometry on no-load losses of medium power transformers. In Proceedings of the International Interdisciplinary PhD Workshop (IIPhDW), Świnoujście, Poland, 9–12 May 2018; pp. 123–127.
10. Kahveci, A.; Szary, P.; Herget, F.; Putri, A.K.; Hameyer, K. Methods for hysteresis losses determinations at non-standard ring core geometries equivalent to epstein measurements. In Proceedings of the 6th International Electric Drives Production Conference (EDPC), Nuremberg, Germany, 30 November–1 December 2016; pp. 135–142.
11. Wang, L.; Huang, I.; Prokhorov, A.V. Different shapes and dimensions of laminated core on characteristics of a practical single-phase distribution transformer using finite-element analysis. In Proceedings of the IEEE Industry Applications Society Annual Meeting, Cincinnati, OH, USA, 1–5 October 2017; pp. 1–9.
12. Puskarczyk, M.; Jamieson, B.; Jurczak, W. The influence of Core Shape and Material Nonlinearities to Corner Losses of Inductive Element. In Proceedings of the 2013 COMSOL Conference, Rotherdam, The Netherlands, 23–25 October 2013.
13. Luo, M.; Dujić, D. Permeance based modelling of the core corners considering magnetic material nonlinearity. In Proceedings of the IECON 2015—41st Annual Conference of the IEEE Industrial Electronics Society, Yokohama, Japan, 9–12 November 2015.
14. Islam, M.R.; Guo, Y.G.; Zhu, J.G. An amorphous alloy core medium frequency magnetic-link for medium voltage photovoltaic inverters. *J. Appl. Phys.* **2014**, *115*, 17E710. [CrossRef]
15. Wei, S.; Fei, W.; Boroyevich, D.; Tipton, C.W. High-density nanocrystalline core transformer for high power high-frequency resonant converter. *IEEE Trans. Ind. Appl.* **2008**, *44*, 213–222.
16. Alyozbaky, O. The losses and temperature comparison in three-phase distribution transformer with various assembly core designs. *Aust. J. Electr. Electron. Eng.* **2018**, *15*, 1–10. [CrossRef]
17. Yehui, H.; Grace, C. Evaluation of magnetic materials for very high frequency power applications. *IEEE Trans. Power Electron.* **2011**, *27*, 425–435.

18. Salvador, K.; Harmel, D.; Oliveira, L.; Cabral, S.; Almaguer, H. Study of the Effectiveness of Magnetic Shielding for Compact Power Transformers Used on Mobile Applications. *IEEE Lat. Am. Trans.* **2020**, *18*, 1034–1040. [CrossRef]
19. Chen, J.; Ma, J.; Fang, Y. An Improved Steinmetz Premagnetization Graph (SPG) Applied in High Magnetic Field. In Proceedings of the 22nd International Conference on Electrical Machines and Systems (ICEMS), Harbin, China, 11–14 August 2019; pp. 1–5.
20. Ionita, V.; Petrescu, L.; Cazacu, E. Impact of Steinmetz Coefficients Variance for FeSi Laminate Magnetic Cores. In Proceedings of the International Symposium on Fundamentals of Electrical Engineering (ISFEE), Bucharest, Romania, 1–3 November 2018; pp. 1–4.
21. Du YCheng, Z.; Xie, D.; Yan, W. Multi-directional magnetic performance simulation of anisotropically oriented silicon steel sheets. *High Volt. Eng.* **2009**, *35*, 3022–3026.
22. He, R.; Zhang, Y.; Zhang, D.; Xie, D. An Improvement of Core Losses Estimation Model in Power Electronic Transformer. In Proceedings of the IEEE Student Conference on Electric Machines and Systems, HuZhou, China, 14–16 December 2018; pp. 1–5.
23. Cao, L.; He, J.; Zhang, B. Model and verification of dynamic hysteresis loss of power transformer core under DC bias magnetic state. *Proc. CSEE* **2008**, *28*, 141–146.
24. Li, Y.; Zhu, L.; Zhu, J. Core Loss Calculation Based on Finite-Element Method with Jiles–Atherton Dynamic Hysteresis Model. *IEEE Trans. Magn.* **2018**, *54*, 1–5. [CrossRef]
25. Zhang, C.; Gao, S.; Zhou, L.; Jiang, J.; Cai, J. Novel Analytical Formulas for Eddy-Current Losses in Semicircle-Section Wound Core of Transformer. *IEEE Trans. Magn.* **2019**, *55*, 1–12. [CrossRef]
26. Guihua, M.; Yancun, L.; Mansheng, G. Study of transformer's harmonic characteristic in DC magnetic bias. In Proceedings of the China International Conference on Electricity Distribution, Guangzhou, China, 10–13 December 2008; pp. 1–4.
27. Ouyang, Z.; Thomsen, O.C.; Andersen, M.A.E. Optimal Design and Tradeoff Analysis of Planar Transformer in High-Power DC–DC Converters. *IEEE Trans. Ind. Electron.* **2012**, *59*, 2800–2810. [CrossRef]
28. Quinn, C.; Rinne, K.; O'Donnell, T.; Duffy, M.; Mathuna, C.O. A review of planar magnetic techniques and technologies. In Proceedings of the Sixteenth Annual IEEE Applied Power Electronics Conference and Exposition, Anaheim, CA, USA, 4–8 March 2001; Volume 2, pp. 1175–1183.
29. Tsai, T.H.; Kuo, L.S.; Chen, P.H.; Lee, D.S.; Yang, C.T. Applications of Ferro-Nanofluid on a Micro-Transformer. *Sensors* **2010**, *10*, 8161–8172. [CrossRef] [PubMed]
30. Yunas, J.; Hamzah, A.; Majlis, B. Surface micromachined on-chip transformer fabricated on glass substrate. *Microsyst. Technol.* **2009**, *15*, 547–552. [CrossRef]
31. Zhao, J.H.; Zhu, J.; Chen, Z.M.; Liu, Z.W. Radio-frequency planar integrated inductor with permalloy-SiO2 granular films. *IEEE Trans. Magn.* **2005**, *41*, 2334–2338. [CrossRef]
32. Tsai, T.H.; Chen, P.H.; Lee, D.S.; Yang, C.T. Investigation of electrical and magnetic properties of ferro-nanofluid on transformers. *Nanoscale Res. Lett.* **2011**, *6*, 264. [CrossRef] [PubMed]
33. Morega, A.M.; Morega, M.; Dimitru, J.B. Magnetic Field-Flow Interactions in a Miniature Electric Power Transformer with Magnetic Nanofluid Core and Solenoid Type Coils. *Rev. Roum. Sci. Tech. Electrotechn. Et. Energ.* **2013**, *58*, 25–34.
34. Kartaca, K.; Abbasov, T.; Karadag, T.; Ekici, Y.; Dikmen, I. Manyetiksıvı Nüveli Transformatörün Tasarımı ve İncelenmesi. In Proceedings of the International Conference on Artificial Intelligence and Data Processing (IDAP), Malatya, Turkey, 28–30 September 2018. [CrossRef]
35. Pîslaru-Dănescu, L.; Morega, A.M.; Dumitru, J.B.; Morega, M.; Popa, N.C.; Stoian, F.D.; Susan-Resiga, D.; Holotescu, S.; Popa, M. Miniature Planar Spiral Transformer with Hybrid, Ferrite, and Magnetic Nanofluid Core. *IEEE Trans. Magn.* **2018**, *54*, 1–14. [CrossRef]